SIAM J. NUMER. ANAL.
Vol. 42, No. 6, pp. 2496–2521

EXPLICIT AND AVERAGING A POSTERIORI ERROR ESTIMATES FOR ADAPTIVE FINITE VOLUME METHODS*

C. CARSTENSEN†, R. LAZAROV‡, AND S. TOMOV§

Abstract. Local mesh-refining algorithms known from adaptive finite element methods are adopted for locally conservative and monotone finite volume discretizations of boundary value problems for steady-state convection-diffusion-reaction equations. The paper establishes residual-type explicit error estimators and averaging techniques for a posteriori finite volume error control with and without upwind in global H^1- and L^2-norms. Reliability and efficiency are verified theoretically and confirmed empirically with experimental support for the superiority of the suggested adaptive mesh-refining algorithms over uniform mesh refining. A discussion of adaptive computations in the simulation of contaminant concentration in a nonhomogeneous water reservoir concludes the paper.

Key words. convection-diffusion-reaction equations, 3-D problems, finite volume approximation, a posteriori error estimators, residual estimators, averaging estimators, ZZ refinement indicator

AMS subject classifications. 65N30, 65M35

DOI. 10.1137/S0036142903425422

1. Introduction.

We consider the following convection-diffusion-reaction problem: Find $u = u(x)$ such that

$$\begin{cases} Lu \equiv \nabla \cdot (-A\nabla u + \underline{b}u) + \gamma u = f & \text{in } \Omega, \\ u = 0 & \text{on } \Gamma_D, \\ (-A\nabla u + \underline{b}u) \cdot \underline{n} = g & \text{on } \Gamma_N^{\text{in}}, \\ -(A\nabla u) \cdot \underline{n} = 0 & \text{on } \Gamma_N^{\text{out}}. \end{cases} \tag{1.1}$$

Here Ω is a bounded polygonal domain in R^d, $d = 2, 3$; $A = A(x)$ is $d \times d$ symmetric, bounded, and uniformly positive definite matrix in Ω; $\underline{b}$ is a given vector function; $\underline{n}$ is the unit outer vector normal to $\partial\Omega$; and f is a given source function. We have also used the notation ∇u for the gradient of a scalar function u and $\nabla \cdot \underline{b}$ for the divergence of a vector function $\underline{b}$ in R^d. The boundary of Ω, $\partial\Omega$ is split into Dirichlet, Γ_D and Neumann, Γ_N parts. Further, the Neumann boundary is divided into two parts: $\Gamma_N = \Gamma_N^{\text{in}} \cup \Gamma_N^{\text{out}}$, where $\Gamma_N^{\text{in}} = \{x \in \Gamma_N : \underline{n}(x) \cdot \underline{b}(x) < 0\}$ and $\Gamma_N^{\text{out}} = \{x \in \Gamma_N : \underline{n}(x) \cdot \underline{b}(x) \geq 0\}$. We assume that Γ_D has positive surface measure.

This problem is a prototype for flow and transport in porous media. For example, $u(x)$ can represent the pressure head in an aquifer or the concentration of a chemical that is dissolved and distributed in groundwater due to the processes of diffusion, dispersion, and absorption. In many cases $A = \epsilon I$, where I is the identity matrix in

*Received by the editors April 1, 2003; accepted for publication (in revised form) May 27, 2004; published electronically March 31, 2005. This work was partially supported by NSF grant DMS–9973328. It was finalized while the first author was a guest at the Isaac Newton Institute for Mathematical Science, Cambridge, UK.

http://www.siam.org/journals/sinum/42-6/42542.html

†Institute of Mathematics, Humboldt University of Berlin, S172: Rudower Chausee 25, Unter den Linden 6, 1099 Berlin, Germany (cc@math.hu-berlin.de).

‡Department of Mathematics, Texas A&M University, College Station, TX 77843-3368 (lazarov@math.tamu.edu).

§Information Technology Division, Brookhaven National Laboratory, Bldg. 515, Upton, NY 11973 (tomov@bnl.gov).

R^d and $\epsilon > 0$ is a small parameter. This corresponds to the important and difficult class of singularly perturbed convection-diffusion problems (see, e.g., the monograph of Ross, Stynes, and Tobiska [31]). In our computations we have used our approach for grid adaptation for this type of problem as well. However, we do not claim that the developed theory in this paper covers this important practical case. Further, $u(x)$ can be viewed as a limit for $t = \infty$ of the solution $u = u(x,t)$ of the corresponding time-dependent problem

$$u_t + Lu = f,\ t > 0,\ x \in \Omega \tag{1.2}$$

with boundary conditions as above and an initial condition $u(x,0) = u_0(x)$, where u_0 is a given function in Ω. Various generalizations, mostly considering nonlinear terms, are possible and widely used in the applications. For example, γu is replaced by a nonlinear reaction term $\gamma(u)$, or the linear convective term $\underline{b}u$ is replaced by a nonlinear flux $\underline{b}(u)$. In this work we follow the framework of the model problem (1.1) and focus on its 3-D setting.

The development of efficient solution methods featuring error control is important for various applications. Our study has been motivated by the research in groundwater modeling and petroleum reservoir simulations (see, e.g., [19]). The solutions of problems in that area exhibit steep gradients and rapid changes due to localized boundary data, discontinuities in the coefficients of the differential equation, and/or other local phenomena (for example, extraction/injection wells, faults, etc.). In order to accurately resolve such local behavior, the numerical method should be able to detect the regions in which the solution changes significantly and to refine the grid locally in a balanced manner so that the overall accuracy is uniform in the whole domain.

Equation (1.1) expresses conservation of the properly scaled quantity u over any subdomain contained in Ω. In the context of groundwater, fluid flow $u(x)$ is in general either the water mass or the mass of the chemical dissolved in the water. Numerical methods that have this property over a number of nonoverlapping subdomains that cover the whole domain are called locally conservative. Finite volumes (control volumes, box schemes), mixed finite elements, and discontinuous Galerkin methods have this highly desirable property. The simplicity of the finite volume approximations combined with their local conservation property and flexibility motivated our study.

There are few works related to a posteriori error estimates for finite volume methods. In [2] Angermann studied a balanced a posteriori error estimate for finite volume discretizations for convection-diffusion equations in two dimensions on Voronoi meshes. The derivation of the error estimator is based on the idea of his previous work [3] on the finite element method. The estimator for the finite volume method contains two new terms which have been studied previously. Some extensions to Angermann's work related to more general situations in respect to space dimension and type of control volumes can be found in Thiele's dissertation [35]. Again, the ideas from the finite element method were exploited in deriving an upper error estimate for the space discretization of parabolic problems. In our paper we use a similar approach; namely, the error estimates for the finite volume method are derived by using the relation between the finite volume and finite element methods (see, e.g., [8]). We note that, despite recent progress (see, e.g., the monographs [23, 26]), the theory of finite volume methods is still under development. This in turn raises certain difficulties in establishing an independent and sharp a posteriori error analysis for the finite volume approximations.

A posteriori error indicators and estimators for the finite element method have been used and studied in the past two decades. Since the pioneering paper of Babuška and Rheinboldt [6], the research in this field has expanded in various directions that include the *residual-based* method (see the survey paper of Verfürth [36]), *hierarchical-based* error estimators [9], estimators based on postprocessing of the approximate solution gradient [37, 38], error estimators that control the error or its gradient in the maximum norm, etc. One popular approach is to evaluate certain local residuals and obtain the a posteriori error indicator by solving local Dirichlet or Neumann problems by taking the local residuals as data [6, 9]. Another variation of the method that controls the global L^2- and H^1-norms of the error uses the Galerkin orthogonality, a priori interpolation estimates, and global stability (see, for example, [21]). Furthermore, solving appropriate dual problems, instead of using the a priori interpolation estimates, leads to error estimators controlling various kinds of error functionals [11]. Solving finite element problems in a space enriched by hierarchical bases functions gives rise to *hierarchical-based* error estimators [9]. There are error estimators based on optimal a priori estimates in a maximum norm [22]. Another type of error estimator/indicator, widely (and in most cases heuristically) used in many adaptive finite element codes, is based on postprocessing (averaging) of the approximate solution gradient (see [37, 38]). In the context of the finite element method for elliptic partial differential equations, averaging or recovery techniques are justified in [10, 14, 30]. Finally, for an extensive study of the efficiency and the reliability of the local estimators and indicators for finite element approximations, we refer to the recent monograph of Babuska and Strouboulis [7].

In this paper we adapt the finite element local error estimation techniques to the case of finite volume approximations. We consider mainly the *residual-based* a posteriori error estimators and analyze the one that uses Galerkin orthogonality, a priori interpolation estimates, and global stability in L^2- and H^1-norms. Our theoretical and experimental findings are similar to those in [2] and could be summarized as follows. The a posteriori error estimates in the finite volume element method are quite close to those in the finite element method, and the mathematical tools from finite element theory can be successfully applied for their analysis. Our computational experiments with various model problems confirm this conclusion. For more computational examples we refer to [25].

The paper is organized as follows. We start with the finite volume element formulation in section 2. The section defines the used notation and approximations and gives some general results from the finite volume approximations. Section 3 studies the *residual-based* error estimator, followed by a short description of the used adaptive refinement strategy (in section 4). Finally, in section 5, we present numerous computational results for 2-D and 3-D test problems which illustrate the adaptive strategy and support our theoretical findings.

2. Finite volume element approximation. Subsection 2.1 introduces the notation used in the paper. In subsection 2.2 we define the finite volume element approximations and give an a priori estimate for the error.

2.1. Notation. We denote by $L^2(K)$ the square-integrable real-valued functions over $K \subset \Omega$, by $(\cdot,\cdot)_{L^2(K)}$ the inner product in $L^2(K)$, and by $|\cdot|_{H^1(K)}$ and $||\cdot||_{H^1(K)}$, respectively, the seminorm and norm of the Sobolev space $H^1(K)$, namely,

$$||u||_{L^2(K)} := (u,u)^{1/2}_{L^2(K)}, \qquad |u|_{H^1(K)} := (\nabla u, \nabla u)^{1/2}_{L^2(K)},$$
$$||u||^2_{H^1(K)} := ||u||^2_{L^2(K)} + |u|^2_{H^1(K)}.$$

In addition, if $K = \Omega$, we suppress the index K and also write $(\cdot,\cdot)_{L^2(\Omega)} := (\cdot,\cdot)$ and $||\cdot||_{L^2} := ||\cdot||$. Further, we use the Hilbert space $H^1_D(\Omega) = \{v \in H^1(\Omega) :\ v|_{\Gamma_D} = 0\}$. Finally, we denote by $H^{1/2}(\partial K)$ the space of the traces of functions in $H^1(K)$ on the boundary ∂K.

To avoid writing unknown constants we use the notation $a \lesssim b$ instead of the inequality $a \le Cb$, where the constant C is independent of the mesh size h.

In our analysis we shall use the following simple inequality valid for $\Omega \subset R^d$, $d > 1$, with Lipschitz continuous boundary $\partial\Omega$ (called Ilin's inequality; cf., e.g., [28]): Let Ω_δ be a strip along $\partial\Omega$ of width δ. Then

$$
\begin{aligned}
&||u||_{L^2(\Omega_\delta)} \lesssim \delta^{1/2}||u||_{H^1(\Omega)} \quad \text{for all } u \in H^1(\Omega);\\
&||u||_{L^2(\Omega_\delta)} \lesssim \delta^{s}||u||_{H^s(\Omega)} \quad \text{for all } u \in H^s(\Omega),\ 0 < s < 1/2.
\end{aligned}
\tag{2.1}
$$

The first inequality is trivial in the case where Ω is a half-space and u has a compact support. The proof in the general case will follow easily by using partition of unity and transforming each subdomain into half-space. The second inequality is obtained using the fact that $||u||_{L^2(\Omega_\delta)} \lesssim \delta||u||_{H^1(\Omega)}$ for all $u \in H^1_0(\Omega)$ and interpolation of Banach spaces (cf., e.g., [1]).

Next, we introduce the bilinear form $a(\cdot,\cdot)$ defined on $H^1_D(\Omega) \times H^1_D(\Omega)$ as

$$
a(u,v) := (A\nabla u - \underline{b}u, \nabla v) + (\gamma u, v) + \int_{\Gamma_N^{\text{out}}} \underline{b}\cdot\underline{n}\ u\ v\, ds. \tag{2.2}
$$

We assume that the coefficients of problem (1.1) are such that

(a) the form is $H^1_D(\Omega)$-elliptic (coercive); i.e., there is a constant $c_0 > 0$ such that

$$
c_0||u||_{H^1} \le a(u,u) \quad \text{for all } u \in H^1_D(\Omega); \tag{2.3}
$$

(b) the form is bounded (continuous) on $H^1_D(\Omega)$; i.e., there is a constant $c_1 > 0$ such that

$$
a(u,v) \le c_1||u||_{H^1}||v||_{H^1} \quad \text{for all } u,\ v \in H^1_D(\Omega). \tag{2.4}
$$

The above two conditions guarantee that the expression $a(u,u)$ is equivalent to the norm in $H^1_D(\Omega)$. Further, we shall use the notation $||u||_a^2 = a(u,u)$ and call this expression the "energy" norm.

A sufficient condition for the coercivity of the bilinear form is $\gamma(x)+0.5\nabla\cdot\underline{b}(x) \ge 0$ for all $x \in \Omega$, while a sufficient condition for the continuity is boundedness of the coefficients $A(x)$, $\underline{b}(x)$, and $\gamma(x)$ in Ω. Further in the paper we assume that these conditions are satisfied. Then (1.1) has the following weak form: Find $u \in H^1_D(\Omega)$ such that

$$
a(u,v) = F(v) := (f,v) - \int_{\Gamma_N^{\text{in}}} gv\, ds \quad \text{for all } v \in H^1_D(\Omega). \tag{2.5}
$$

2.2. Approximation method. The domain Ω is partitioned into triangular (for the 2-D case) or tetrahedral (for the 3-D case) finite elements denoted by K. The

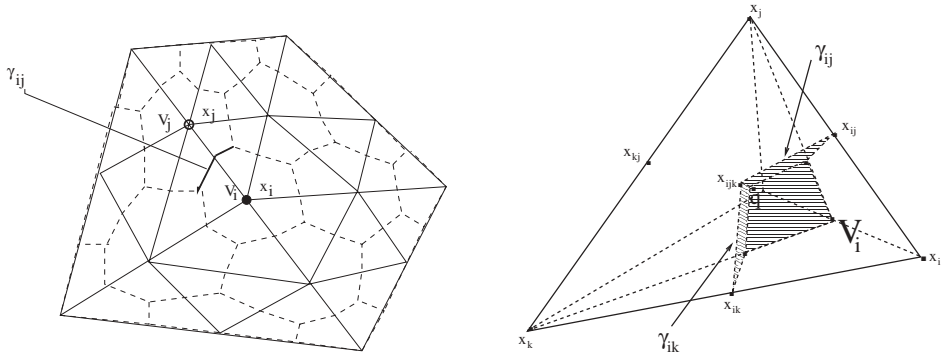

FIG. 1. *Left: Finite element and finite volume partitions in two dimensions. Right: Contribution from one element to control volume V_i, γ_{ij}, and γ_{ik} in three dimensions; point q is the element's medicenter. Internal points for the faces are the medicenters of the faces.*

elements are considered to be closed sets and the splitting, often called triangulation of Ω, is denoted by $\mathcal{T}$. We assume that the mesh is aligned with the discontinuities of the coefficients of the differential equation (if any), with the data f and g, and with the interfaces between Γ_D, Γ_N^{out}, and Γ_N^{in}.

We note that our analysis will be valid also for domains with smooth boundaries. In this case we have to modify the triangulation so that the methods do not lose accuracy due to approximation of the domain. Such schemes have been discussed in [18].

We introduce the set $N_h = \{x_i : x_i \text{ is a vertex of element } K \in \mathcal{T}\}$ and denote by N_h^0 the set of all vertices in N_h except those on Γ_D. For a given vertex x_i we denote by $\Pi(i)$ the index set of all neighbors of x_i in N_h, i.e., all vertices that are connected to x_i by an edge.

For a given finite element triangulation $\mathcal{T}$, we construct a dual mesh $\mathcal{T}^*$ (based upon $\mathcal{T}$), whose elements are called control volumes (boxes, finite volumes, etc.). There are various ways to introduce the control volumes. Almost all approaches can be described in the following general scheme. In each element $K \in \mathcal{T}$ a point q is selected. For the 3-D case, on each of the four faces $\overline{x_i x_j x_k}$ of K a point x_{ijk} is selected and on each of the six edges $\overline{x_i x_j}$ a point x_{ij} is selected. Then q is connected to the points x_{ijk}, and in the corresponding faces, the points x_{ijk}, are connected to the points x_{ij} by straight lines (see Figure 1). Control volume associated with a vertex x_i is denoted by V_i and defined as the union of the "quarter" elements $K \in \mathcal{T}$, which have x_i as a vertex (see Figure 1). The interface between two control volumes, V_i and V_j, is denoted by γ_{ij}, i.e., $\overline{V}_i \cap \overline{V}_j = \gamma_{ij}$.

We assume that $\mathcal{T}$ is locally quasi uniform, that is, for $K \in \mathcal{T}$, $|K| \lesssim \rho(K)^d$, where $\rho(K)$ is the radius of the largest ball contained in K and $|K|$ denotes the area or volume of K. In the context of locally refined grids, this means that the smallest interior angle is bounded away from zero and any two neighboring finite elements are of approximately the same size, whereas elements that are far away may have quite different sizes.

In our 3-D computations q is the center of gravity of the element K, x_{ijk} are the centers of gravity of the corresponding faces, and x_{ij} are the mid-points (centers of gravity) of the corresponding edges (as shown on Figure 1).

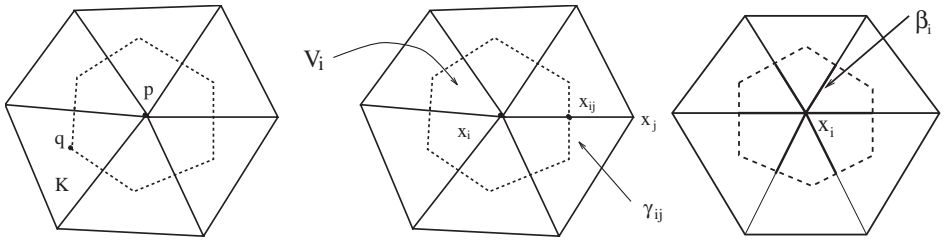

FIG. 2. *Control volumes with circumcenters as internal points (Voronoi meshes) and interface γ_{ij} of V_i and V_j. The rightmost picture shows the segments β_i in bold.*

In two dimensions, another possibility is to choose q to be the center of the circumscribed circle of K. These types of control volumes form Voronoi or perpendicular bisector (PEBI) meshes (see, e.g. [23, pp. 764, 825]). Then obviously, γ_{ij} are the PEBIs of the three edges of K (see Figure 2). This construction requires that all finite elements are triangles of acute type, which we shall assume whenever such triangulation is used.

We define the linear finite element space S_h as

$$S_h = \{v \in C(\Omega) : v|_K \text{ is affine for all } K \in \mathcal{T} \text{ and } v|_{\Gamma_D} = 0\}$$

and its dual volume element space S_h^* by

$$S_h^* = \{v \in L^2(\Omega) : v|_V \text{ is constant for all } V \in \mathcal{T}^* \text{ and } v|_{\Gamma_D} = 0\}.$$

Obviously, $S_h = \text{span}\{\phi_i : x_i \in N_h^0\}$ and $S_h^* = \text{span}\{\chi_i : x_i \in N_h^0\}$, where ϕ_i denotes the standard nodal linear basis function associated with the node x_i, and χ_i denotes the characteristic function of the volume V_i. Let $I_h : C(\Omega) \cap H_D^1(\Omega) \to S_h$ be the interpolation operator and $I_h^* : C(\Omega) \cap H_D^1(\Omega) \to S_h^*$ and $P_h^* : C(\Omega) \cap H_D^1(\Omega) \to S_h^*$ be the piecewise constant interpolation and projection operators:

$$I_h u = \sum_{x_i \in N_h} u(x_i)\phi_i(x),\ I_h^* u = \sum_{x_i \in N_h} u(x_i)\chi_i(x),\ \text{and } P_h^* u = \sum_{x_i \in N_h} \bar{u}_i \chi_i(x).$$

Here $\bar{u}_i$ is the averaged value of u over the volume V_i for $x_i \in N_h^0$, i.e., $\bar{u}_i = \int_{V_i} u\,dx/|V_i|$, and $\bar{u}_i = 0$ for $x_i \in \Gamma_D$. In fact, I_h also makes sense as an interpolation operator from S_h^* to S_h. Namely, if $v^* \in S_h^*$, then $I_h v^* \in S_h$ and $I_h v^*(x_i) = v^*(x_i)$.

Further, for $v^* \in S_h^*$, we use the notation $v_i^* = v^*(x_i)$. We also define the "total flux" and its approximation by

$$\underline{\sigma} := -A\nabla u + \underline{b}u, \qquad \underline{\sigma}_h := -A\nabla_h u_h + \underline{b}u_h$$

and assume that the coefficients $A(x)$ and $\underline{b}(x)$ are elementwise smooth. Also, we denote by $\nabla_h \cdot$ the $\mathcal{T}$-piecewise divergence and by ∇_h the $\mathcal{T}$-piecewise gradient. Integrals involving piecewise quantities are considered as sums over the pieces where the quantities are defined.

The finite volume element approximation u_h of (1.1) is the solution to the following problem: Find $u_h \in S_h$ such that

$$a_h(u_h, v_h^*) := A(u_h, v_h^*) + C(u_h, v_h^*) = F(v_h^*) \quad \text{for all } v_h^* \in S_h^*. \tag{2.6}$$

Here the bilinear forms $A(u_h, v^*)$ and $C(u_h, v^*)$ are defined on $S_h \times S_h^*$ and the linear form $F(v^*)$ is defined on S_h^*. They are given by

$$A(u_h, v^*) = \sum_{x_i \in N_h^0} v_i^* \left(- \int_{\partial V_i \setminus \Gamma_N} (A \nabla_h u_h) \cdot \underline{n} ds + \int_{V_i} \gamma u_h dx \right), \tag{2.7}$$

$$C(u_h, v^*) = \sum_{x_i \in N_h^0} v_i^* \int_{\partial V_i \setminus \Gamma_N^{\text{in}}} (\underline{b} \cdot \underline{n})\ u_h \, ds, \tag{2.8}$$

$$F(v^*) = \sum_{x_i \in N_h^0} v_i^* \left\{ \int_{V_i} f dx - \int_{\partial V_i \cap \Gamma_N^{\text{in}}} g \, ds \right\}. \tag{2.9}$$

Obviously, $\nabla \cdot \underline{\sigma}_h$ is well defined over $V_i \cap K$ for all $V_i \in \mathcal{T}^*$ and $K \in \mathcal{T}$. This ensures, in particular, that the surface integrals in (2.7) and (2.8) exist.

In addition to $C(u_h, v^*)$ we introduce the form $C^{\text{up}}(u_h, v^*)$ that uses upwind approximation. Approximation (2.7)–(2.9) can be used for moderate convection fields and dominating diffusion. For small diffusion, for example, when $A = \epsilon I$ with ϵ small, approximation (2.7)–(2.9) gives oscillating numerical results, which we would like to avoid. We are interested in approximation methods that produce solutions satisfying the maximum principle and are locally conservative. Such schemes are also known as monotone schemes (see, e.g., [24, 31]). A well-known sufficient condition for a scheme to be monotone is that the corresponding stiffness matrix be an M-matrix (see [33, pp. 182, 260] and [31, p. 202]).

The upwind approximation that we use for problems with large convection (or small diffusion) is locally mass conservative and gives the desired stabilization. We split the integral over ∂V_i on integrals over $\gamma_{ij} = \partial V_i \cap \partial V_j$ (see Figure 1) and introduce out-flow and in-flow parts of the boundary of the volume V_i. This splitting can be characterized by the quantities $(\underline{b} \cdot \underline{n})_+ = \max(0,\ \underline{b} \cdot \underline{n})$ and $(\underline{b} \cdot \underline{n})_- = \min(0,\ \underline{b} \cdot \underline{n})$, where $\underline{n}$ is the outer unit vector normal to ∂V_i. Then we introduce

$$C^{\text{up}}(u_h, v^*) = \sum_{x_i \in N_h^0} v_i^* \Bigg\{ \sum_{j \in \Pi(i)} \int_{\gamma_{ij}} \left((\underline{b} \cdot \underline{n})_+ u_h(x_i) + (\underline{b} \cdot \underline{n})_- u_h(x_j) \right) ds + \int_{\Gamma_N^{\text{out}} \cap \partial V_i} (\underline{b} \cdot \underline{n})\, u_h(x_i)\ ds \Bigg\}. \tag{2.10}$$

This approximation is well defined for any $\underline{b}$. In order to avoid technicalities in our analysis we assume that the vector field $\underline{b}$ is piecewise smooth and has small variation over each finite element. Thus, the quantity $\underline{b} \cdot \underline{n}$ does not change sign over γ_{ij}.

The upwind finite volume element approximation u_h of (1.1) becomes the following: Find $u_h \in S_h$ such that

$$a_h^{\text{up}}(u_h, v^*) := A(u_h, v^*) + C^{\text{up}}(u_h, v^*) = F(v^*) \text{ for all } v^* \in S_h^*. \tag{2.11}$$

This is an extension of the classical upwind approximation of the convection term and is closely related to the discontinuous Galerkin approximation (see, e.g., [22]) or to the Tabata scheme for the Galerkin finite element method [34]. It is also related to the scheme on Voronoi meshes derived by Mishev [27]. A different type of weighted upwind approximation on Voronoi meshes in two dimensions has been studied by Angermann [2].

3. A posteriori error analysis. This section is devoted to the mathematical derivation of computable error bounds in the energy norm. Throughout this section, $u \in H^1_D$ denotes the exact solution of (2.5) and $u_h \in S_h$ denotes the discrete solution of either (2.6) or (2.11). Then, $e := u - u_h \in H^1_D(\Omega)$ is the (unknown) error and $\overline{e} := P^*_h e \in S^*_h$ is its $\mathcal{T}^*$-piecewise integral mean. We denote by $\mathcal{E}$ the set of all interior edges/faces in $\mathcal{T}$, respectively, in two/three dimensions. Also, for a vertex $x_i \in N^0_h$ let $\beta_i := V_i \cap \mathcal{E}$ (see Figure 2). For any $E \in \mathcal{E}$ let $[\underline{\sigma}_h] \cdot \underline{n}$ denote the jump of $\underline{\sigma}_h$ across E in normal to E direction $\underline{n}$. The orientation of $\underline{n}$ is not important as long as the jump is in the same direction. In general, if $\underline{n}$ is present in a boundary integral, it will denote the outward unit vector normal to the boundary. With every element $K \in \mathcal{T}$, edge/face $E \in \mathcal{E}$, and volume $V_i \in \mathcal{T}^*$ we associate local mesh size denoted correspondingly by h_K, h_E, and h_i. Since the mesh is locally quasi uniform the introduced mesh sizes are locally equivalent, i.e., bound each other from above and below with constants independent of the mesh size. Then, we introduce a global discontinuous mesh size function $h(x)$, $x \in \Omega$, that assumes value h_K, h_E, and h_i depending on $x \in K \setminus \partial K$, $x \in E$, or $x = x_i$, respectively. Finally, we use the following shorthand notation for integration over all faces E in $\mathcal{E}$:

$$\int_{\mathcal{E}} v ds := \sum_{E \in \mathcal{E}} \int_E v ds, \qquad \|v\|_{L^2(\mathcal{E})} := \sum_{E \in \mathcal{E}} \int_E v^2 ds.$$

3.1. Energy-norm a posteriori error estimate of the scheme without upwind. We consider problem (2.6) and begin our analysis with the case when the form $C(\cdot,\cdot)$ is evaluated by (2.8). We first give a representation of the error and introduce some locally computable quantities. In Theorem 3.1 we show that these quantities give a reliable estimate for the error. Further, we introduce the error estimator, based on local "averaging" of the "total flux" $\underline{\sigma}$ over the control volumes, and show that this estimator is reliable up to higher order terms.

The following lemma gives a representation of the error.

LEMMA 3.1. *Assume that the bilinear form $a(\cdot,\cdot)$ satisfies* (2.3) *and* (2.4). *Then for the error $e = u - u_h$, where u is the solution of* (2.5) *and u_h is the solution of* (2.6), *we have*

$$\begin{aligned} \|e\|_a^2 &= (f - \nabla_h \cdot \underline{\sigma}_h - \gamma u_h,\ e - \overline{e}) - \int_{\mathcal{E}} [\underline{\sigma}_h] \cdot \underline{n}\, (e - \overline{e})\, ds \\ &\quad - \int_{\Gamma_N^{\mathrm{in}}} (g - \underline{\sigma}_h \cdot \underline{n})\, (e - \overline{e})\, ds - \int_{\Gamma_N^{\mathrm{out}}} (A \nabla_h u_h) \cdot \underline{n}\, (e - \overline{e})\, ds. \end{aligned} \tag{3.1}$$

Proof. We take $v = e \in H^1_D(\Omega)$ in (2.5) and use the definition of $a(\cdot,\cdot)$ by (2.2) to get

$$\begin{aligned} a(e,e) &= a(u,e) - a(u_h,e) \\ &= (f - \gamma u_h, e) + (\underline{\sigma}_h, \nabla e) - \int_{\Gamma_N^{\mathrm{in}}} g e\, ds - \int_{\Gamma_N^{\mathrm{out}}} (\underline{b} \cdot \underline{n})\, u_h\, e\, ds. \end{aligned}$$

We integrate the second term on the right-hand side by parts on each element $K \in \mathcal{T}$:

$$\int_K \underline{\sigma}_h \cdot \nabla e\, ds = \int_{\partial K} (\underline{\sigma}_h \cdot \underline{n}) e\, ds - \int_K e \nabla \cdot \underline{\sigma}_h\, dx.$$

The sum over all elements yields the jump contributions $[\underline{\sigma}_h]\cdot\underline{n}$ along $\mathcal{E}$ and eventually proves

$$
\begin{aligned}
a(e,e) &= (f-\nabla_h\cdot\underline{\sigma}_h-\gamma u_h,e)-\int_{\mathcal{E}}[\underline{\sigma}_h]\cdot\underline{n}\,e\,ds\\
&\quad-\int_{\Gamma_N^{\mathrm{in}}}(g-\underline{\sigma}_h\cdot\underline{n})e\,ds-\int_{\Gamma_N^{\mathrm{out}}}(A\nabla_h u_h)\cdot\underline{n}\,e\,ds.
\end{aligned}
\tag{3.2}
$$

It remains to be shown that the preceding right-hand side vanishes if e is replaced by $\overline{e}$. For each control volume V_i we have from (2.6)–(2.8) that

$$
\int_{\partial V_i\setminus\Gamma_N}\underline{\sigma}_h\cdot\underline{n}\,ds=\int_{V_i}(f-\gamma u_h)\,dx-\int_{\partial V_i\cap\Gamma_N^{\mathrm{out}}}(\underline{b}\cdot\underline{n})\,u_h\,ds-\int_{\partial V_i\cap\Gamma_N^{\mathrm{in}}}g\,ds.
$$

The Gauss divergence theorem is applied to each nonvoid $K\cap V_i$, $K\in\mathcal{T}$, so that the left-hand side of the above inequality becomes

$$
\int_{\partial V_i\setminus\Gamma_N}\underline{\sigma}_h\cdot\underline{n}\,ds=\int_{V_i}\nabla_h\cdot\underline{\sigma}_h\,dx+\int_{\beta_i}[\underline{\sigma}_h]\cdot\underline{n}\,ds-\int_{\partial V_i\cap\Gamma_N}\underline{\sigma}_h\cdot\underline{n}\,ds.
$$

The difference of the preceding two identities is multiplied by $\overline{e}(x_i)$ and summed over all control volumes. This results in

$$
0=(f-\nabla_h\cdot\underline{\sigma}_h-\gamma u_h,\overline{e})-\int_{\mathcal{E}}[\underline{\sigma}_h]\cdot\underline{n}\,\overline{e}\,ds-\int_{\Gamma_N^{\mathrm{in}}}(g-\underline{\sigma}_h\cdot\underline{n})\,\overline{e}\,ds-\int_{\Gamma_N^{\mathrm{out}}}A\nabla_h u_h\cdot\underline{n}\,\overline{e}\,ds.
$$

Subtracting this identity from (3.2) concludes the proof of (3.1). ∎

Motivated by the above considerations we introduce the following locally computable quantities that play a major role in the design of adaptive algorithms and their a posteriori error analysis.

DEFINITION 3.1. *Set*

$$
\begin{aligned}
R_K(x)&:=(f-\nabla\cdot\underline{\sigma}_h-\gamma u_h)(x),\ x\in K,\\
R_E(x)&:=([\underline{\sigma}_h]\cdot\underline{n})(x),\ x\in E,\ \textit{for } E\cap\Gamma_N=\emptyset,\\
R_E^{\mathrm{in}}(x)&:=(g-\underline{\sigma}_h\cdot\underline{n})(x),\ x\in E,\ \textit{for } E\subset\Gamma_N^{\mathrm{in}},\\
R_E^{\mathrm{out}}(x)&:=(A\nabla u_h\cdot\underline{n})(x),\ x\in E,\ \textit{for } E\subset\Gamma_N^{\mathrm{out}}
\end{aligned}
$$

and define

$$
\begin{aligned}
\eta_R&:=\|h\,R_K\|_{L^2(\Omega)},\ \eta_E:=\|h^{1/2}\,R_E\|_{L^2(\mathcal{E})},\\
\eta_N&:=\|h^{1/2}\,R_E^{\mathrm{in}}\|_{L^2(\Gamma_N^{in})}+\|h^{1/2}\,R_E^{\mathrm{out}}\|_{L^2(\Gamma_N^{\mathrm{out}})}.
\end{aligned}
$$

LEMMA 3.2. *Suppose that $R_E\in L^2(\mathcal{E})$ and that the partitioning $\mathcal{T}$ of Ω is locally quasi uniform. Then*

$$
\int_{\mathcal{E}}[\underline{\sigma}_h]\cdot\underline{n}(e-\overline{e})\,ds\lesssim\eta_E\,\|\nabla e\|\ \textit{for any } e\in H^1_D(\Omega),
$$

where the constant in the notation $\lesssim$ depends only on the shape of the elements in $\mathcal{T}$ and the volumes in $\mathcal{T}^*$.

Proof. A well-established trace inequality (cf., e.g., [12, Theorem 1.6.6] or [15, Theorem 1.4]) and scaling argument lead to

$$h_E^{1/2}\|v\|_{L^2(E)} \lesssim \|v\|_{L^2(K)} + h_E\|\nabla v\|_{L^2(K)} \tag{3.3}$$

for all $v \in H^1(K)$ and edges E of an element $K \in \mathcal{T}$. An application to $v := e - \overline{e}$ on each $K \cap V_i$, where $K \in \mathcal{T}$ and $x_i \in N_h$, leads to

$$\begin{aligned}\int_{\beta_i} [\underline{\sigma}_h]\cdot\underline{n}(e-\overline{e})\,ds &\le \|[\underline{\sigma}_h]\cdot\underline{n}\|_{L^2(\beta_i)}\|e-\overline{e}\|_{L^2(\beta_i)}\\ &\lesssim h_i^{1/2}\|[\underline{\sigma}_h]\cdot\underline{n}\|_{L^2(\beta_i)}(h_i^{-1}\|e-\overline{e}\|_{L^2(V_i)} + \|\nabla e\|_{L^2(V_i)}).\end{aligned}$$

Further, Poincaré's inequality for $x_i \in N_h^0$ (in which case $\int_{V_i}(e-\overline{e})\,dx = 0$) or Friedrichs's inequality for $x_i \in N_h\backslash N_h^0$ (in which case $\overline{e} = 0$ on V_i and $e = 0$ on $\partial V_i \cap \Gamma_D$) shows that

$$h_i^{-1}\|e-\overline{e}\|_{L^2(V_i)} \lesssim \|\nabla e\|_{L^2(V_i)}. \tag{3.4}$$

Poincaré's, respectively, Friedrichs's, inequality is valid in this case because the volumes V_i are star shaped w.r.t. a ball of radius $\sim h_i$, which follows from the quasi uniformity of $\mathcal{T}$ and our choice of $\mathcal{T}^*$. Substituting the last result into the preceding inequality yields

$$\int_{\beta_i} [\underline{\sigma}_h]\cdot\underline{n}(e-\overline{e})\,ds \lesssim \|h^{1/2}\ [\underline{\sigma}_h]\cdot\underline{n}\|_{L^2(\beta_i)}\|\nabla e\|_{L^2(V_i)}$$

for all $x_i \in N_h$. A summation over all vertices yields the assertion. ∎

Below we establish that the sum of the quantities η_R, η_E, and η_N gives a reliable estimate for the error in the global energy norm.

THEOREM 3.1. *Assume that the coefficients of the bilinear form $a(\cdot,\cdot)$ are such that* (2.3) *and* (2.4) *are satisfied, and that the partitioning $\mathcal{T}$ of Ω is locally quasi uniform. Then*

$$\|e\|_a \lesssim \eta_R + \eta_E + \eta_N.$$

The constant in this inequality depends on the constants c_0 in (2.3) *and c_1 in* (2.4)*, and on the shape of the elements in $\mathcal{T}$ and $\mathcal{T}^*$, but is independent of h.*

Proof. The identity (3.1) of Lemma 3.1 represents $\|e\|_a^2$ as a sum of four terms. We bound the first term using Cauchy's inequality, the second one using Lemma 3.2, and the remaining two terms using again Cauchy's inequality:

$$\|e\|_a^2 \lesssim \eta_R\|h^{-1}(e-\overline{e})\| + \eta_E\|\nabla e\| + \eta_N\|h^{-1/2}(e-\overline{e})\|_{L^2(\Gamma_N)}.$$

Inequality (3.4) is combined with the trace inequality (3.3) to obtain

$$\|h^{-1/2}(e-\overline{e})\|_{L^2(\Gamma_N)}^2 + \|h^{-1}(e-\overline{e})\|^2 \lesssim \sum_{x_i\in N_h}(h_i^{-2}\|e-\overline{e}\|_{L^2(V_i)}^2 + \|\nabla e\|_{L^2(V_i)}^2) \lesssim \|\nabla e\|^2.$$

Condition (2.3) yields $\|\nabla e\| \lesssim \|e\|_a$ and this concludes the proof of the theorem. ∎

Now we introduce an error estimator that is based on local averaging (post-processing) of the "total flux" $\underline{\sigma}_h$. For finite element approximations this estimator,

often called the ZZ-estimator, has been justified by Carstensen and Bartels [10, 14] and Rodriguez [30].

DEFINITION 3.2. *Let P_i be the L^2-projection onto the affine functions on V_i. We define the error indicator η_Z for $A(x)$ and $\underline{b}(x)$ smooth over the volumes $V_i \in \mathcal{T}^*$ as*

$$\eta_Z := \left(\sum_{x_i \in N_h} \|\underline{\sigma}_h - P_i \underline{\sigma}_h\|^2_{L^2(V_i)} \right)^{1/2}.$$

Remark 3.1. In our numerical experiments we have allowed $A(x)$ to have jumps that are aligned with the partition $\mathcal{T}$. In such cases we have changed the projection P_i. For example, if $V_i = V_i^1 \cup V_i^2$ and $A(x)$ is smooth on V_i^1 and V_i^2 but has jumps across their interface, then P_i is defined in a piecewise way as

$$\|\underline{\sigma}_h - P_i \underline{\sigma}_h\|^2_{L^2(V_i)} = \|\underline{\sigma}_h - P_i^1 \underline{\sigma}_h\|^2_{L^2(V_i^1)} + \|\underline{\sigma}_h - P_i^2 \underline{\sigma}_h\|^2_{L^2(V_i^2)},$$

where P_i^1 and P_i^2 are the L^2-projections on the affine functions on V_i^1 and V_i^2, respectively.

To simplify our notation we shall use the concept of "higher order terms" (h.o.t.). Since the finite volume scheme at hand is of first order for $u \in H^2(\Omega)$, i.e., $\|e\|_a \lesssim h$, then it is reasonable to denote all terms that tend to zero faster than $O(h)$ by h.o.t. Below, we shall refer to the following quantities as h.o.t.:

(a) $\|h^2\ \nabla(\gamma u_h)\|_{L^2(\Omega)}$ for $\gamma \in H^1(\Omega)$;
(b) $\|h^2\ \nabla f\|_{L^2(\Omega)}$ if $f \in H^1(\Omega)$;
(c) $\|hf\|_{L^2(\Omega_D)}$ if $f \in H^s(\Omega)$, $s > 0$, and $\Omega_D := \cup\{V_i : x_i \in N_h \cap \Gamma_D\}$ is a strip of width h around Γ_D (to show that this quantity is h.o.t. we apply Ilin's inequality (2.1) and get $\|hf\|_{L^2(\Omega_D)} \lesssim h^{1+s}\|f\|_{H^s(\Omega)}$, $s < 1/2$);
(d) $h_E^{1/2}\|g - \bar{g}\|_{L^2(E)}$ for $\bar{g} = \int_E g ds/|E|$ and $g \in H^1(E)$ for $E \subset \Gamma_N^{\text{out}}$;
(e) denote by $\tilde{r}(x)$ a linear approximation of $r(x)$ on K. Thus, $\widetilde{\nabla \cdot A}$ and $\widetilde{\nabla \cdot \underline{b}}$ are linear approximations on K of $\nabla \cdot A$ and $\nabla \cdot \underline{b}$, respectively. Here $\nabla \cdot A$ is understood as a vector with components divergence of the rows of $A(x)$. If A and $\underline{b}$ are sufficiently smooth on K, then $\nabla \cdot A - \widetilde{\nabla \cdot A}$ and $\nabla \cdot \underline{b} - \widetilde{\nabla \cdot \underline{b}}$ are h.o.t.

More generally, if functions $\alpha(h)$, $\beta(h)$, and $\gamma(h)$ satisfy $\alpha(h) \le \beta(h) + \gamma(h)$ and $\gamma(h)/\beta(h) \to 0$ as $h \to 0$, we will denote $\gamma(h)$ as h.o.t. compared to $\beta(h)$. In the case above we have $\beta(h) = h$.

In the analysis that follows we derive a posteriori error estimates based on averaging techniques. In the estimates derived the constants in $\lesssim$ depend only on c_0 from (2.3), c_1 from (2.4), and the shape of the elements in $\mathcal{T}$ and $\mathcal{T}^*$. The h.o.t. will account for the smoothness of the coefficients of the differential equation. The smoothness requirements, as stated in the theorems below, yield h.o.t. of order $O(h^2)$, i.e., one order higher than needed. Using standard results from interpolation of Banach spaces (cf., e.g., [1]) we can weaken the assumptions, requiring smoothness of order $\epsilon > 0$ less than that stated.

LEMMA 3.3. *Let the coefficients A and $\underline{b}$ be $C^1(\Omega)$-functions and let P_i be the L^2-projection onto the affine functions on $V_i \in \mathcal{T}^*$. Then*

$$h_i^{1/2}\|[\underline{\sigma}_h] \cdot \underline{n}\|_{L^2(\beta_i)} \lesssim \|\underline{\sigma}_h - P_i \underline{\sigma}_h\|_{L^2(V_i)} + \text{h.o.t.} \quad \text{for all } V_i \in \mathcal{T}^*. \tag{3.5}$$

The multiplicative constants in the notation $\lesssim$ depend on the shape of the elements in $\mathcal{T}$ and the shape of the control volumes in $\mathcal{T}^*$, while the h.o.t. depend on the smoothness of the coefficients A and $\underline{b}$.

Proof. If A and $\underline{b}$ are polynomials, then $\underline{\sigma}_h|_K$ is in a finite dimensional space for any $K \in \mathcal{T}$. In this case we easily prove (3.5) without h.o.t. by an equivalence-of-norm argument on finite dimensional spaces. Namely, both sides of (3.5) define seminorms for finite dimensional $\underline{\sigma}_h$. If $\|\underline{\sigma}_h - P_i\underline{\sigma}_h\|_{L^2(V_i)} = 0$ for some $\underline{\sigma}_h$, then $\underline{\sigma}_h = P_i\underline{\sigma}_h$ on V_i. Since $P_i\underline{\sigma}_h$ is linear on V_i, this shows that $\underline{\sigma}_h$ is also linear. Therefore, the jump $[\underline{\sigma}_h]$ is zero on β_i, i.e., the left-hand side of (3.5) vanishes as well. This proves that the seminorm on the right-hand side is stronger than the seminorm on the left-hand side and so proves (3.5). A scaling argument shows that the multiplicative constant behind $\lesssim$ is independent of h_i.

The case when A and $\underline{b}$ are smooth functions but $\underline{\sigma}_h|_K$ is not finite dimensional over $K \in \mathcal{T}$ is treated using approximation. Namely, we introduce polynomial approximations $\overline{\underline{\sigma}}_h$ of $\underline{\sigma}_h$ for any $K \in \mathcal{T}$ based on approximations of A and $\underline{b}$, taking into account that

$$\|\underline{\sigma}_h - \overline{\underline{\sigma}}_h\|_{L^2(V_i)} = \text{h.o.t.} \quad \text{and} \quad \|[\underline{\sigma}_h - \overline{\underline{\sigma}}_h] \cdot \underline{n}\|_{L^2(V_i)} = \text{h.o.t.},$$

and use the result for the finite dimensional case to get (3.5). ∎

As a corollary we get the following inequality.

COROLLARY 3.1. *Let the assumptions of Lemma* 3.3 *be satisfied. Then*

$$\eta_E \lesssim \eta_Z + \textit{h.o.t.} \tag{3.6}$$

The above inequality follows directly by squaring (3.5) and summing over all $x_i \in N_h$.

Recall that η_Z is defined for internal vertex nodes. Below we show that η_Z together with η_N can be used as an estimator for the H^1-norm of the error modulus of h.o.t.

THEOREM 3.2. *Let the assumptions of Lemma* 3.3 *be satisfied and let* $f \in H^1(\Omega)$. *Then*

$$\|e\|_a \lesssim \eta_Z + \eta_N + \textit{h.o.t.} \tag{3.7}$$

Proof. We use again the error representation from Lemma 3.1. In Theorem 3.1 we have bounded the third and fourth sums from the error representation by $\eta_N\|\nabla e\|$ and the second sum by $\eta_E\|\nabla e\|$. Further, η_E was bounded in Lemma 3.3 by η_Z + h.o.t., so it remains to establish the bound

$$(f - \nabla \cdot \underline{\sigma}_h - \gamma u_h,\ e - \overline{e}) \lesssim (\eta_Z + \text{h.o.t.})\|\nabla e\|.$$

For $x_i \in N_h^0$ denote by $\overline{f}$ and $\overline{\gamma u_h}$ the integral means over V_i of f and γu_h, respectively. Then we have

$$\begin{aligned}\int_{V_i} (f - \nabla_h \cdot \underline{\sigma}_h - \gamma u_h)(e - \overline{e})\,dx &= \int_{V_i} (f - \overline{f})(e - \overline{e})\,dx \\ &\quad - \int_{V_i} \nabla_h \cdot (\underline{\sigma}_h - P_i\underline{\sigma}_h)(e - \overline{e})\,dx - \int_{V_i} (\gamma u_h - \overline{\gamma u_h})(e - \overline{e})\,dx \\ &\le \|e - \overline{e}\|_{L^2(V_i)}\big(\|f - \overline{f}\|_{L^2(V_i)} + \|\nabla_h \cdot (\underline{\sigma}_h - P_i\underline{\sigma}_h)\|_{L^2(V_i)} \\ &\qquad + \|\gamma u_h - \overline{\gamma u_h}\|_{L^2(V_i)}\big).\end{aligned} \tag{3.8}$$

Poincaré's inequality gives

$$\begin{aligned}\|e - \overline{e}\|_{L^2(V_i)} &\lesssim h_i\|\nabla e\|_{L^2(V_i)}, \\ \|f - \overline{f}\|_{L^2(V_i)} &\lesssim h_i\|\nabla f\|_{L^2(V_i)}, \\ \|\gamma u_h - \overline{\gamma u_h}\|_{L^2(V_i)} &\lesssim h_i\|\nabla(\gamma u_h)\|_{L^2(V_i)}.\end{aligned} \tag{3.9}$$

The term $\|\nabla_h \cdot (\underline{\sigma}_h - P_i\underline{\sigma}_h)\|_{L^2(V_i)}$ is treated by the inverse estimate

$$\|\nabla_h \cdot (\underline{\sigma}_h - P_i\underline{\sigma}_h)\|_{L^2(V_i)} \lesssim h_i^{-1}\|\underline{\sigma}_h - P_i\underline{\sigma}_h\|_{L^2(V_i)} + \text{h.o.t.} \tag{3.10}$$

As in the proof of Lemma 3.3, we first prove (3.10) when $\underline{\sigma}_h$ is finite dimensional by equivalence of norms followed by a scaling argument and then, for the general case, by a perturbation analysis. The combination of (3.8)–(3.10) shows

$$\int_{V_i} (f - \nabla_h \cdot \underline{\sigma}_h - \gamma u_h)(e - \overline{e})\, dx \lesssim \|\nabla e\|_{L^2(V_i)} \left(\|\underline{\sigma}_h - P_i\underline{\sigma}_h\|_{L^2(V_i)} + \text{h.o.t.}\right). \tag{3.11}$$

So far (3.11) holds for $x_i \in N_h^0$. For $x_i \in N_h \cap \Gamma_D$ we replace $\overline{e}$, $\overline{f}$, and $\overline{\gamma u_h}$ by zero and deduce the first and third inequalities of (3.9) from Friedrichs's inequality (notice that e and γu_h vanish on $\Gamma_D \cap V_i$). The inverse estimate (3.10) holds for $x_i \in N_h \cap \Gamma_D$ as well. The aforementioned arguments prove (3.11) with $\|h^2\ \nabla f\|_{L^2(V_i)}$ replaced by $\|h\, f\|_{L^2(V_i)}$. This shows

$$(f - \nabla_h \cdot \underline{\sigma}_h - \gamma u_h, e - \overline{e}) \lesssim (\eta_Z + \|hf\|_{L^2(\Omega_D)} + \text{h.o.t.})\|\nabla e\|.$$

The last result, the discussion at the beginning of the theorem, Ilin's inequality (2.1), and the ellipticity assumption conclude the proof of the theorem. ∎

THEOREM 3.3. *Suppose that the coefficients A and $\underline{b}$ are $C^1(\Omega)$-functions, $f \in H^1(\Omega)$, $\gamma \in H^1(\Omega)$, $g \in H^{1/2}(\mathcal{E})$, and that the partitioning $\mathcal{T}$ of Ω is locally quasi uniform. Then*

$$\eta_Z + \eta_R + \eta_E + \eta_N \lesssim \|e\|_a + h.o.t.$$

Proof. We will prove that the quantities η_R, η_E, η_N, and η_Z are bounded by $C\ \|e\|_a + \text{h.o.t.}$ The h.o.t. appear by applying averaging techniques as in the proof of Lemma 3.3 and therefore we will consider only the case when $\underline{\sigma}_h$ is finite dimensional. First, we will bound the contributions to η_N due to Γ_N^{in}, namely, we will prove

$$\|h^{1/2}\,(g - \underline{\sigma}_h \cdot \underline{n})\|_{L^2(\Gamma_N^{\text{in}})} \lesssim \|e\|_a + \text{h.o.t.} \tag{3.12}$$

We consider an element $K \in \mathcal{T}$ that has an edge/face $E \subset \Gamma_N^{\text{in}}$. We will use the pair (K, E) in the rest of the proof (see Figure 3).

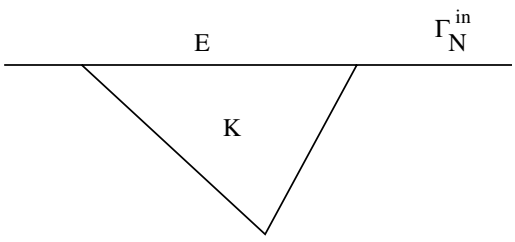

FIG. 3. *The pair (K, E) of edge $E \subset \Gamma_N^{\text{in}}$ and element K used in the proof of inequality* (3.12).

First, we note that

$$h_E^{1/2}\|g-\overline{g}\|_{L^2(E)} = \text{h.o.t.} \quad \text{for} \quad \overline{g} := \int_E g\,ds/|E|.$$

Then

$$\|g-\underline{\sigma}_h\cdot\underline{n}\|_{L^2(E)} \le \|g-\overline{g}\|_{L^2(E)} + \|\overline{g}-\underline{\sigma}_h\cdot\underline{n}\|_{L^2(E)} \lesssim \|\overline{g}-\underline{\sigma}_h\cdot\underline{n}\|_{L^2(E)} + \text{h.o.t.}$$

We prove below that

$$\|\overline{g}-\underline{\sigma}_h\cdot\underline{n}\|_{L^2(E)} \lesssim h_E^{-1/2}\|\underline{\sigma}-\underline{\sigma}_h\|_{L^2(K)} + \text{h.o.t.}$$

so that summation over all $E\subset\Gamma_N^{\text{in}}$ yields (3.12).

Consider an edge-bubble function $b_E\in H^1(\Omega)$, $b_E\ge 0$, $b_E(x)=0$ on $\Omega\setminus K$ and $\partial K\setminus E$, with properties

$$\int_E b_E\,ds = \int_E ds,\ \|b_E\|_{L^\infty(K)}\lesssim 1,\ \|\nabla b_E\|_{L^\infty(K)}\lesssim 1/h_E. \tag{3.13}$$

A 2-D example of such a bubble is $b_E = 6\phi_1\phi_2$, where ϕ_1 and ϕ_2 are the standard linear nodal basis functions associated with the end points of the edge E. Let $z\in H^1(K)$ be the harmonic extension of $(\overline{g}-\underline{\sigma}_h\cdot\underline{n})b_E$ from ∂K to K. The extension is bounded in H^1 [29, Theorem 4.1.1] on a reference element $\hat{K}$ by the $H^{1/2}(\hat{E})$-norm of the extended quantity and, since all norms are equivalent on a finite dimensional space, by its $L^2(\hat{E})$-norm. Therefore, a scaling argument gives

$$h_E^{1/2}\|\nabla z\|_{L^2(K)} + h_E^{-1/2}\|z\|_{L^2(K)} \lesssim \|b_E(\overline{g}-\underline{\sigma}_h\cdot\underline{n})\|_{L^2(E)}. \tag{3.14}$$

We define the linear operator P_K into the space of polynomials of degree 2 on an element $K\in\mathcal{T}$ as

$$(b_K\ P_K z, p_h)_{L^2(K)} = (z,p_h)_{L^2(K)}$$

for all polynomials p_h of degree 2. Here $b_K\in H^1(\Omega)$, $b_K\ge 0$, is an element-bubble function with properties

$$\text{supp } b_K\subset K,\ \int_K b_K\,ds = \int_K ds,\ \|b_K\|_{L^\infty(K)}\lesssim 1,\ \|\nabla b_K\|_{L^\infty(K)}\lesssim 1/h_K.$$

A 2-D example of such a bubble is $b_K = 60\phi_1\phi_2\phi_3$, where ϕ_1, ϕ_2, and ϕ_3 are the standard linear nodal basis functions associated with the vertices of the element K. Then $\tilde{z} := z - b_K\,P_K z$ by construction has the properties

$$\tilde{z} = (\overline{g}-\underline{\sigma}_h\cdot\underline{n})b_E \quad \text{on } E, \qquad \tilde{z}=0 \quad \text{on } \partial K\backslash E,$$
$$(\tilde{z},\,p_h)_{L^2(K)} = 0 \quad \text{for all polynomials } p_h \text{ of degree 2.}$$

Inequality (3.14) remains valid for z replaced by $\tilde{z}$ because of the following. Choosing $p_h = P_K z$ in the definition of P_K yields

$$\|b_K^{1/2}P_K z\|_{L^2(K)}^2 = (z,P_K z)_{L^2(K)} \lesssim \|z\|_{L^2(K)}\|P_K z\|_{L^2(K)}.$$

We use norm equivalence on finite dimensional spaces on a reference element and scaling to K to get that the quantities $||b_K P_K z||_{L^2(K)}$, $\|b_K^{1/2}P_K z\|_{L^2(K)}$, and $\|P_K z\|_{L^2(K)}$

are equivalent up to constants independent of h, and therefore $\|b_K P_K z\|_{L^2(K)} \lesssim \|z\|_{L^2(K)}$. We use again the equivalence-of-norms argument, inverse inequality, and the properties of z to get that

$$\begin{aligned}\|\nabla(b_K P_K z)\|_{L^2(K)} &\lesssim \|\nabla b_K\|_{L^2(K)}\|P_K z\|_{L^2(K)} + \|b_K \nabla(P_K z)\|_{L^2(K)}\\ &\lesssim h_E^{-1}\|P_K z\|_{L^2(K)} + h_E^{-1}\|z\|_{L^2(K)}\\ &\lesssim h_E^{-1/2}\|b_E(\overline{g} - \underline{\sigma}_h\cdot\underline{n})\|_{L^2(E)}.\end{aligned}$$

Combined with the bound for $\|b_K P_K z\|_{L^2(K)}$, this completes the proof of (3.12) for $z = \tilde{z}$.

Given a polynomial p_h of degree 2, using the Gauss divergence theorem and the properties of $\tilde{z}$, we deduce

$$\begin{aligned}&\int_E b_E(\overline{g} - \underline{\sigma}_h\cdot\underline{n})(\underline{\sigma} - \underline{\sigma}_h)\cdot\underline{n}\,ds = \int_{\partial K}\tilde{z}(\underline{\sigma} - \underline{\sigma}_h)\cdot\underline{n}\,ds\\ &\quad= \int_K(\underline{\sigma} - \underline{\sigma}_h)\cdot\nabla\tilde{z}\,dx + \int_K \tilde{z}(\nabla\cdot(\underline{\sigma} - \underline{\sigma}_h) - p_h)\,dx\\ &\quad\lesssim \big(\|\underline{\sigma} - \underline{\sigma}_h\|_{L^2(K)} + h_E\|\nabla\cdot(\underline{\sigma} - \underline{\sigma}_h) - p_h\|_{L^2(K)}\big)\, h_E^{-1/2}\|b_E(\overline{g} - \underline{\sigma}_h\cdot\underline{n})\|_{L^2(E)}.\end{aligned}$$

Choosing proper p_h in the second term of the last inequality makes that term h.o.t. Indeed, write down first the equality (see the basic problem (1.1))

$$\nabla\cdot(\underline{\sigma} - \underline{\sigma}_h) - p_h = \gamma u - f - (\nabla\cdot A)\cdot\nabla u_h + u_h\,\nabla\cdot\underline{b} + \underline{b}\cdot\nabla u_h - p_h. \tag{3.15}$$

Here $\nabla\cdot A$ is understood as a vector with component divergence on the rows of $A(x)$. Let $\tilde{f}$, $\widetilde{\gamma u}$, $\widetilde{\nabla\cdot\underline{b}}$, $\tilde{\underline{b}}$, and $\widetilde{\nabla\cdot A}$ be the linear approximations on K of f, γu, $\nabla\cdot\underline{b}$, $\underline{b}$, and $\nabla\cdot A$, respectively.

Now, we choose p_h to be the following polynomial of degree 2 on K,

$$p_h = \widetilde{\gamma u} - \tilde{f} - (\widetilde{\nabla\cdot A})\cdot\nabla u_h + u_h\widetilde{\nabla\cdot\underline{b}} + \tilde{\underline{b}}\cdot\nabla u_h,$$

take the $L^2(K)$-norm of (3.15), and use the triangle's inequality to get

$$\begin{aligned}\|\nabla\cdot(\sigma - \underline{\sigma}_h) - p_h\|_{L^2(K)} &\le \|f - \tilde{f}\|_{L^2(K)} + \|\gamma u - \widetilde{\gamma u}\|_{L^2(K)} + \|u_h(\nabla\cdot\underline{b} - \widetilde{\nabla\cdot\underline{b}})\|_{L^2(K)}\\ &\quad + \|(\underline{b} - \tilde{\underline{b}})\cdot\nabla u_h\|_{L^2(K)} + \|\nabla u_h\cdot(\nabla\cdot A - \widetilde{\nabla\cdot A})\|_{L^2(K)}\\ &\lesssim \big(\|u\|_{H^2(K)} + \|u_h\|_{H^1(K)}\big)\ \text{h.o.t.} + \|h_K\nabla f\|_{L^2(K)}.\end{aligned}$$

Therefore (note that $g = \underline{\sigma}\cdot\underline{n}$ on Γ_N^{in}),

$$\begin{aligned}\|b_E^{1/2}(\overline{g} - \underline{\sigma}_h\cdot\underline{n})\|_{L^2(E)}^2 &= \int_E \tilde{z}(\overline{g} - g)\,ds + \int_E\tilde{z}(\underline{\sigma} - \underline{\sigma}_h)\cdot\underline{n}\,ds\\ &\lesssim h_E^{-1/2}\big(\|\underline{\sigma} - \underline{\sigma}_h\|_{L^2(K)} + \text{h.o.t.}\big)\ \|b_E^{1/2}(\overline{g} - \underline{\sigma}_h\cdot\underline{n})\|_{L^2(E)}\end{aligned}$$

and so

$$\|b_E^{1/2}(\overline{g} - \underline{\sigma}_h\cdot\underline{n})\|_{L^2(E)} \lesssim h_E^{-1/2}\|\underline{\sigma} - \underline{\sigma}_h\|_{L^2(K)} + \text{h.o.t.}$$

Using again the equivalence-of-norms estimate (equivalence of norms on finite dimensional spaces on reference element and scaling)

$$\|\overline{g} - \underline{\sigma}_h\cdot\underline{n}\|_{L^2(E)} \lesssim \|b_E^{1/2}(\overline{g} - \underline{\sigma}_h\cdot\underline{n})\|_{L^2(E)}$$

we finally prove that

$$\begin{aligned}\|g-\underline{\sigma}_h\cdot\underline{n}\|_{L^2(E)} &\le \|g-\overline{g}\|_{L^2(E)}+\|\overline{g}-\underline{\sigma}_h\cdot\underline{n}\|_{L^2(E)}\\ &\lesssim \|b_E^{1/2}(\overline{g}-\underline{\sigma}_h\cdot\underline{n})\|_{L^2(E)}+\text{h.o.t.}\\ &\lesssim h_E^{-1/2}\|\underline{\sigma}-\underline{\sigma}_h\|_{L^2(K)}+\text{h.o.t.}\end{aligned}$$

Similarly, $\|A\nabla u_h\cdot\underline{n}\|_{L^2(E)}\lesssim h_E^{-1/2}\|\underline{\sigma}-\underline{\sigma}_h\|_{L^2(K)}+\text{h.o.t.}$ for $E\subset\Gamma_N^{\text{out}}$, which, combined with the result for $E\subset\Gamma_N^{\text{in}}$, proves that $\eta_N\lesssim||e||_a+\text{h.o.t.}$

A similar technique shows that $\eta_E\lesssim\|e\|_a+\text{h.o.t.}$

The inequality $\eta_R\lesssim\|e\|_a+\text{h.o.t.}$ can be proved in the following way. Take the average $\bar{R}_K$ of the residual $R_K:=f-\nabla\cdot\underline{\sigma}_h-\gamma u_h$ over an element K to derive

$$\|\bar{R}_K\|_{L^2(K)}\le\|R_K-\bar{R}_K\|_{L^2(K)}+\|R_K\|_{L^2(K)}=\ \text{h.o.t.}+\|R_K\|_{L^2(K)}.$$

Further, apply the technique from Lemma 3.1 to deduce the equality $(R_K,b_K\bar{R}_K)_{L^2(K)}=a(e,b_K\bar{R}_K)$ and therefore

$$\begin{aligned}(R_K,b_K\bar{R}_K)_{L^2(K)}&=\|b_K^{1/2}R_K\|^2_{L^2(K)}-(R_K,b_K(R_K-\bar{R}_K))_{L^2(K)}=a(e,b_K\bar{R}_K)\\ &\lesssim\|e\|_{H^1(K)}\|b_K\bar{R}_K\|_{H^1(K)}\lesssim\|e\|_{H^1(K)}h_K^{-1}\|\bar{R}_K\|_{L^2(K)}\\ &\lesssim h_K^{-1}\|e\|_{H^1(K)}\|R_K\|_{L^2(K)}+\text{h.o.t.}\end{aligned}$$

Here we used the inverse inequality and the boundedness of the coefficients of the differential equation (1.1). Then we take the term $(R_K,b_K(R_K-\bar{R}_K))_{L^2(K)}$ to the right-hand side and consider it as h.o.t. Finally, use that $\|b_K^{1/2}R_K\|_{L^2(K)}\approx\|R_K\|_{L^2(K)}$ to obtain

$$\|R_K\|_{L^2(K)}\lesssim h_K^{-1}\|e\|_{H^1(K)}+\text{h.o.t.}$$

A summation over all $K\in\mathcal{T}$ yields the inequality $\eta_R\lesssim\|e\|_a+\text{h.o.t.}$

Now we prove the remaining inequality, $\eta_Z\lesssim\|e\|_a+\text{h.o.t.}$ Since P_i is a linear $L^2(V_i)$ projector, we have that

$$\|\underline{\sigma}_h-P_i\underline{\sigma}_h\|_{L^2(V_i)}\le\|\underline{\sigma}_h-P_i\underline{\sigma}\|_{L^2(V_i)}.$$

Adding and subtracting $\underline{\sigma}$ in the right-hand side and applying the triangle's inequality we get

$$\|\underline{\sigma}_h-P_i\underline{\sigma}\|_{L^2(V_i)}\le\|\underline{\sigma}_h-\underline{\sigma}\|_{L^2(V_i)}+\|\underline{\sigma}-P_i\underline{\sigma}\|_{L^2(V_i)}=\|\underline{\sigma}_h-\underline{\sigma}\|_{L^2(V_i)}+\text{h.o.t.}$$

since $\|\underline{\sigma}-P_i\underline{\sigma}\|_{L^2(V_i)}=\text{h.o.t.}$ for $\underline{\sigma}$ smooth. The summation over all x_i concludes the proof of the theorem. ∎

3.2. Analysis of the upwind scheme in the H^1-norm. This section is devoted to the case when an upwind approximation is applied to the convection term, namely, we consider problem (2.11).

DEFINITION 3.3. *For an element $K\in\mathcal{T}$ we denote by $\gamma_K:=\cup_{\gamma_{ij}}(K\cap\gamma_{ij})$ and set*

$$\eta_E^{\text{up}}:=\left(\sum_{K\in\mathcal{T}}\sum_{\gamma_{ij}\subset\gamma_K}\|h^{1/2}\underline{b}\cdot\underline{n}\,(u_h(x_i)-u_h)\|^2_{L^2(\gamma_{ij})}\right)^{1/2},$$

$$\eta_N^{\text{up}}:=\|h^{1/2}\underline{b}\cdot\underline{n}\,\nabla u_h\|_{L^2(\Gamma_N^{\text{out}})}.$$

THEOREM 3.4. *Let the assumptions of Theorems* 3.1 *and* 3.2 *be satisfied, and let the upwind approximation be applied to the convection term. Then*

$$\|e\|_a \lesssim \eta_Z + \eta_N + \eta_E^{\mathrm{up}} + \eta_N^{\mathrm{up}} + h.o.t. \tag{3.16}$$

Proof. Since $a_h^{\mathrm{up}}(u_h, v^*) = F(v^*)$ and $a_h(u, v^*) = F(v^*)$ for $v^* \in S_h^*$ we have the orthogonality condition $a_h(u, v^*) - a_h^{\mathrm{up}}(u_h, v^*) = 0$. Choosing $v^* = \bar{e}$ we get the following representation for the energy norm of the error:

$$\begin{aligned}\|e\|_a^2 &= a(e,e) - a_h(u,\bar{e}) + a_h^{\mathrm{up}}(u_h,\bar{e}) \\ &= \{a(e,e) - a_h(e,\bar{e})\} + \{a_h^{\mathrm{up}}(u_h,\bar{e}) - a_h(u_h,\bar{e})\} \\ &= \{a(e,e) - a_h(e,\bar{e})\} + \{C_h^{\mathrm{up}}(u_h,\bar{e}) - C_h(u_h,\bar{e})\}.\end{aligned}$$

For the first term, $a(e,e) - a_h(e,\bar{e})$, we use the same approach as in the analysis of the scheme without upwind (see Lemma 3.1) and show that

$$\begin{aligned}a(e,e) - a_h(u,\bar{e}) &= (f - \nabla_h \cdot \underline{\sigma}_h - \gamma u_h,\ e - \bar{e}) - \int_{\mathcal{E}} [\underline{\sigma}_h] \cdot \underline{n}\,(e - \bar{e})\,ds \\ &\quad - \int_{\Gamma_N^{\mathrm{in}}} (g - \underline{\sigma}_h \cdot \underline{n})\,(e - \bar{e})\,ds - \int_{\Gamma_N^{\mathrm{out}}} (A\nabla_h u_h) \cdot \underline{n}\,(e - \bar{e})\,ds.\end{aligned} \tag{3.17}$$

This presentation allows us to use estimate (3.7) of Theorem 3.2.

For the second term, $C_h^{\mathrm{up}}(u_h,\bar{e}) - C_h(u_h,\bar{e})$, we get

$$\begin{aligned}C_h^{\mathrm{up}}(u_h,\bar{e}) - C_h(u_h,\bar{e}) = \sum_{x_i \in N_h^0} \bar{e}_i \Bigg\{ &\sum_{j \in \Pi(i)} \int_{\gamma_{ij}} ((\underline{b}\cdot\underline{n})_+ u_h(x_i) + (\underline{b}\cdot\underline{n})_- u_h(x_j) - \underline{b}\cdot\underline{n} u_h)\,ds \\ &+ \int_{\partial V_i \cap \Gamma_N^{\mathrm{out}}} (\underline{b}\cdot\underline{n}\ u_h(x_i) - \underline{b}\cdot\underline{n}\ u_h)\ ds \Bigg\}.\end{aligned}$$

Here the unit normal vector $\underline{n}$ on γ_{ij} is oriented in such a way that $\underline{b}\cdot\underline{n} \geq 0$. We want to express the above sum as a sum over the elements. To do so we specify that the indexes (ij) are oriented so that $(x_i - x_j)\cdot\underline{n} \leq 0$. We get that

$$\begin{aligned}C_h^{\mathrm{up}}(u_h,\bar{e}) - C_h(u_h,\bar{e}) = \sum_{K \in \mathcal{T}_h} \Bigg\{ &\sum_{\gamma_{ij} \subset K} (\bar{e}_i - \bar{e}_j) \int_{\gamma_{ij}} \underline{b}\cdot\underline{n}\,(u_h(x_i) - u_h)\,ds \\ &+ \sum_{V_i \cap K} \bar{e}_i \int_{\partial V_i \cap \Gamma_N^{\mathrm{out}}} \underline{b}\cdot\underline{n}\ (u_h(x_i) - u_h)\ ds \Bigg\}.\end{aligned}$$

We denote by $[\bar{e}] := e_i - \bar{e}_j$ the jump of $\bar{e}$ across γ_{ij} and take into account that $[\bar{e} - e] = [\bar{e}]$. Then, by the Schwarz inequality, the term involving the integral over γ_{ij} is bounded by $C\|[e - \bar{e}]\|_{L^2(\gamma_{ij})}\ \|\underline{b}\cdot\underline{n}\,(u_h(x_i) - u_h)\|_{L^2(\gamma_{ij})}$. As before, using trace, Poincaré's, and/or Friedrichs's inequalities we get

$$\|[e - \bar{e}]\|_{L^2(\gamma_{ij})} \lesssim h_i^{1/2} \|\nabla e\|_{L^2(V_i)},$$

which bounds the integrals over γ_{ij} in the error representation with η_E^{up}.

For the terms involving integration over Γ_N^{out} we have

$$|u_h(x_i) - u_h(x)| \leq |\nabla u_h \cdot \underline{t}(x)|.|x_i - x|.$$

Here $\underline{t}(x)$ is a unit vector along $\partial V_i \cap K$, an edge in two dimensions, or a face in three dimensions. Then in two dimensions $\underline{t}$ is simply a unit vector perpendicular to $\underline{n}$, while in three dimensions $\underline{t}(x)$ depends on the position of x on the face and is again perpendicular to $\underline{n}$. In both cases $|u_h(x_i) - u_h(x)| \leq |h_K \nabla u_h|$. Using the Schwarz inequality we bound the term involving integration over Γ_N^{out} in the following way:

$$\sum_{V_i \cap K} \bar{e}_i \int_{\partial V_i \cap \Gamma_N^{\text{out}}} \underline{b} \cdot \underline{n}\, (u_h(x_i) - u_h)\, ds \leq C \|\nabla e\|.\|h^{1/2} \underline{b} \cdot \underline{n}\, \nabla u_h\|_{L^2(\Gamma_N^{\text{out}})},$$

which eventually gives the term η_N^{up} in (3.16) and completes the proof. ∎

3.3. Error estimates in L^2. We use duality techniques to get error estimators for different quantities of the error. In this subsection we will show how to use the duality technique in order to derive an error estimator in the global $L^2(\Omega)$-norm for the scheme without upwinding. The main assumption in this section is that the solution of problem (1.1) is H^2 regular.

DEFINITION 3.4. *We define the residual L^2 a posteriori error estimator $\tilde{\rho}$ as*

$$\tilde{\rho} := (\tilde{\eta}_R^2 + \tilde{\eta}_E^2 + \tilde{\eta}_N^2)^{1/2}, \tag{3.18}$$

where

$$\begin{aligned}
\tilde{\eta}_R^2 &:= \|h\,(R_K - \bar{R}_K)\|^2 + \|h^2\, R_K\|^2, \\
\tilde{\eta}_E^2 &:= \|h^{1/2}\,(R_E - \bar{R}_E)\|_{L^2(\mathcal{E})}^2 + \|h^{3/2}\, R_E\|_{L^2(\mathcal{E})}^2, \\
\tilde{\eta}_N^2 &:= \|h^{1/2}\,(R_E^{\text{in}} - \bar{R}_E^{\text{in}})\|_{L^2(\Gamma_N^{\text{in}})}^2 + \|h^{3/2}\, R_E^{\text{in}}\|_{L^2(\Gamma_N^{\text{in}})}^2 \\
&\quad + \|h^{1/2}\,(R_E^{\text{out}} - \bar{R}_E^{\text{out}})\|_{L^2(\Gamma_N^{\text{out}})}^2 + \|h^{3/2}\, R_E^{\text{out}}\|_{L^2(\Gamma_N^{\text{out}})}^2,
\end{aligned}$$

and $\bar{R}_K$, $\bar{R}_E$, $\bar{R}_E^{\text{in}}$, and $\bar{R}_E^{\text{out}}$ are the $K \in \mathcal{T}$, $E \in \mathcal{E}$, $E \in \Gamma_N^{\text{in}}$, and $E \in \Gamma_N^{\text{out}}$ piecewise mean values of, correspondingly, R_K, R_E, R_E^{in}, and R_E^{out} introduced in Definition 3.1.

Our aim is to show that the estimator $\tilde{\rho}$ is reliable in the $L^2(\Omega)$-norm. The a posteriori $L^2(\Omega)$ error analysis involves the following continuous dual problem: Find $\tilde{e} \in H_D^1(\Omega)$ such that

$$a(v, \tilde{e}) = (e, v) \text{ for any } v \in H_D^1(\Omega), \tag{3.19}$$

where e is the exact error, defined as before.

THEOREM 3.5. *Let the solution $\tilde{e}$ of the dual problem* (3.19) *be $H^2(\Omega)$ regular. If the coefficients of our basic problem* (1.1) *are sufficiently regular, namely R_K, R_E, R_E^{in}, and R_E^{out} are correspondingly in $H^1(K)$, $H^{1/2}(E)$, $H^{1/2}(\Gamma_N^{\text{in}})$, and $H^{1/2}(\Gamma_N^{\text{out}})$, then the residual L^2 a posteriori error estimator* (3.18) *from Definition* 3.4 *is reliable, i.e., $\|e\| \lesssim \tilde{\rho}$.*

Proof. Let $v = e$ in (3.19) and argue as in the proof of Lemma 3.1 to show

$$\begin{aligned}
\|e\|^2 = a(e, \tilde{e}) &= (R_K, \tilde{e} - e^*) - (R_E, \tilde{e} - e^*)_{L^2(\mathcal{E})} \\
&\quad - (R_E^{\text{in}}, \tilde{e} - e^*)_{L^2(\Gamma_N^{\text{in}})} - (R_E^{\text{out}}, \tilde{e} - e^*)_{L^2(\Gamma_N^{\text{out}})}
\end{aligned} \tag{3.20}$$

for an arbitrary $e^* \in S_h^*$. To evaluate the right-hand side of this identity we use the nodal interpolation operator I_h and its properties. If $\tilde{e} \in H^2(\Omega)$, the Sobolev inequalities [12, Theorem 4.3.4] guarantee that $I_h\tilde{e}$ is well defined. The properties of the interpolant are well established in the finite element literature (see, for example, [12]), namely,

(3.21)
$$h_K^{-2}\|\tilde{e} - I_h\tilde{e}\|_{L^2(K)} + h_K^{-1}|\tilde{e} - I_h\tilde{e}|_{H^1(K)} + h_K^{-3/2}\|\tilde{e} - I_h\tilde{e}\|_{L^2(\partial K)} \leq C_{I,K}|\tilde{e}|_{H^2(K)}.$$

Now, in (3.20) we choose $e^* = I_h^* I_h\tilde{e}$ so that $\tilde{e} - e^* = (\tilde{e} - I_h\tilde{e}) + (I_h\tilde{e} - I_h^* I_h\tilde{e})$. Further, we apply the Schwarz inequality on the integrals involving $\tilde{e} - I_h\tilde{e}$ and use (3.21) to get the bound

$$\begin{aligned}(R_K, \tilde{e} - I_h\tilde{e}) - (R_E, \tilde{e} - I_h\tilde{e})_{L^2(\mathcal{E})} - (R_E^{\text{in}}, \tilde{e} - I_h\tilde{e})_{L^2(\Gamma_N^{\text{in}})} - (R_E^{\text{out}}, \tilde{e} - I_h\tilde{e})_{L^2(\Gamma_N^{\text{out}})}\\ \lesssim \big(\|h^2\ R_K\| + \|h^{3/2}\ R_E\|_{L^2(\mathcal{E})} + \|h^{3/2}\ R_E^{\text{in}}\|_{L^2(\Gamma_N^{\text{in}})} + \|h^{3/2}\ R_E^{\text{out}}\|_{L^2(\Gamma_N^{\text{out}})}\big)|\tilde{e}|_{H^2(\Omega)}.\end{aligned}$$

For the integrals involving $I_h\tilde{e} - I_h^* I_h\tilde{e}$ we first note that if K is a fixed element in $\mathcal{T}$, then for every vertex x_i of K, the quantities $|K \cap V_i|$ (volume in three dimensions and area in two dimensions) are equal. Also, for vertices x_i on the face/edge E we have that the boundary quantities $|E \cap V_i|$ (area in three dimensions and length in two dimensions) are also equal. Therefore,

$$\int_K (I_h\tilde{e} - I_h^* I_h\tilde{e})dx = 0, \qquad \int_E (I_h\tilde{e} - I_h^* I_h\tilde{e})ds = 0.$$

We apply the last fact to the integrals involving $I_h\tilde{e} - I_h^* I_h\tilde{e}$ in order to subtract from R_K, R_E, R_E^{in}, and R_E^{out} their mean values $\bar{R}_K$, $\bar{R}_E$, $\bar{R}_E^{\text{in}}$, and $\bar{R}_E^{\text{out}}$. Then, using Schwarz and Poincaré inequalities we bound the term involving $I_h\tilde{e} - I_h^* I_h\tilde{e}$, namely,

$$\begin{aligned}&|(R_K, I_h^* I_h\tilde{e} - I_h\tilde{e}) - (R_E, I_h^* I_h\tilde{e} - I_h\tilde{e})_{L^2(\mathcal{E})} - (R_E^{\text{in}}, I_h^* I_h\tilde{e} - I_h\tilde{e})_{L^2(\Gamma_N^{\text{in}})}\\ &\qquad - (R_E^{\text{out}}, I_h^* I_h\tilde{e} - I_h\tilde{e})_{L^2(\Gamma_N^{\text{out}})}|\\ &\lesssim \big(\|h\ (R_K - \bar{R}_K)\| + \|h^{1/2}(R_E - \bar{R}_E)\|_{L^2(\mathcal{E})}\\ &\qquad + \|h^{1/2}\ (R_E^{\text{in}} - \bar{R}_E^{\text{in}})\|_{L^2(\Gamma_N^{\text{in}})} + \|h^{1/2}\ (R_E^{\text{out}} - \bar{R}_E^{\text{out}})\|_{L^2(\Gamma_N^{\text{out}})}\big)\|\tilde{e}\|_{H^2(K)},\end{aligned}$$

where we have used the inequality

$$\begin{aligned}\|I_h\tilde{e} - I_h^* I_h\tilde{e}\|_{L^2(K)} &\lesssim h_K|I_h\tilde{e}|_{H^1(K)} \lesssim h_K|\tilde{e} - I_h\tilde{e}|_{H^1(K)} + h_K|\tilde{e}|_{H^1(K)}\\ &\lesssim h_K^2|\tilde{e}|_{H^2(K)} + h_K|\tilde{e}|_{H^1(K)} \lesssim h_K|\tilde{e}|_{H^2(K)}.\end{aligned}$$

Applying the above estimates, the stability of the dual problem with respect to the right-hand side, $\|\tilde{e}\|_{H^2(\Omega)} \leq C\|e\|$, and obvious manipulations, we get that the L^2 a posteriori error estimator $\tilde{\rho}$ is reliable. Moreover, since the coefficients of (1.1) are sufficiently regular we can apply Poincaré's inequality to the terms $\|R_K - \bar{R}_K\|_{L^2(K)}$, $\|R_E - \bar{R}_E\|_{L^2(E)}$, $\|R_E^{\text{in}} - \bar{R}_E^{\text{in}}\|_{L^2(E)}$, and $\|R_E^{\text{out}} - \bar{R}_E^{\text{out}}\|_{L^2(E)}$ to get one additional power of h that will make the error estimator of second order.

Note that we did not explicitly apply Poincaré's inequality in the definition of the error estimator in order to make it well defined for problems with less than that stated in the theorem regularity. ∎

4. Adaptive grid refinement and solution strategy. In this section we present the adaptive mesh refinement strategy that we use. It is based on the grid refinement approach in the finite element methods (see, e.g., [11, 36]). A different grid adaptation strategy, again in the finite element method, has been proposed, justified, and used in [20].

For a given finite element partitioning $\mathcal{T}$, desired error tolerance ρ, and a norm in which the tolerance to be achieved is, say $|||\cdot|||$, do the following:

- compute the finite volume approximation $u_h \in S_h$, as given in subsection 2.2;
- using the a posteriori error analysis, compute the errors ρ_K for all $K \in \mathcal{T}$;
- mark those finite elements K for which $\rho_K \geq \rho/\sqrt{N}$; here N is the number of elements in $\mathcal{T}$;
- if $\sum_{K\in\mathcal{T}} \rho_K^2 > \rho^2$, then refine the marked elements;
- additionally refine until a conforming mesh is reached;
- repeat the above process until no elements have been refined.

For the 2-D case we refine marked elements by uniformly splitting the marked triangles into four. The refinement to conformity is done by bisection through the longest edge. For the 3-D version of the code the elements (tetrahedrons) are refined using the algorithm described by Arnold, Mukherjee, and Pouly in [5].

The described procedure yields error control and optimal mesh (heuristics), which are the goals in the adaptive algorithm. The nested meshes obtained in the process are used to define multilevel preconditioners. The initial guess for every new level is taken to be the interpolation of u_h from the previous level.

5. Numerical examples. Here we present two sets of numerical examples to test the our theoretical results. The first two examples are simple 2-D elliptic problems while the remaining tests illustrate our approach on 3-D problems of flow and transport in porous media.

5.1. 2-D test problems. In Example 1 we consider problems with known solutions and compare the behavior of the error estimators with the exact errors. Example 2 is for discontinuous matrix $A(x)$ with an unknown solution.

Example 1. We consider three Dirichlet problems for the Poisson equation on an L-shaped domain with known exact solutions $u = r^{4/3}\sin\frac{4\theta}{3}$ (Problem 1), $u = r^{2/3}\sin\frac{2\theta}{3}$ (Problem 2), and $u = r^{1/2}\sin\frac{\theta}{2}$ (Problem 3). These functions belong to $H^{1+s}(\Omega)$ with s almost $4/3$, $2/3$, and $1/2$, respectively. In Figure 4 we show the mesh and the error for Problem 2 after four levels of local refinement.

The theory shows that the a posteriori error estimators η_E and η_Z are equivalent to the H^1-norm of the error. This theoretical result is confirmed by our computations, which are summarized in Figure 5. The left picture gives the exact error (solid line) and the a posteriori error estimators η_Z (dashed line) and η_E (dash-dotted line) for the three problems over the different levels of the mesh. The levels are obtained by uniform refinement (splitting every triangle into 4) and have 65, 255, 833, 3,201, 12,545, 49,665, and 197,633 nodes correspondingly for levels $1, \ldots, 7$. The errors are printed in logarithmic scale in order to demonstrate the linear behavior of the error as a function of the level. For exact solutions in $H^{1+1/2-\epsilon}$, $H^{1+2/3-\epsilon}$, and $H^{1+4/3-\epsilon}$ ($\epsilon > 0$) one can see the theoretically expected rate of error reduction over the levels of $1/2$, $2/3$, and 1 correspondingly. One can observe that both η_Z and η_E are equivalent to the exact error, as proved in the theoretical section. The same is true when the local refinement method from section 4 is applied. The numerical results are given in Figure 5, right. The y scale is again the error, and the x scale is the refinement level.

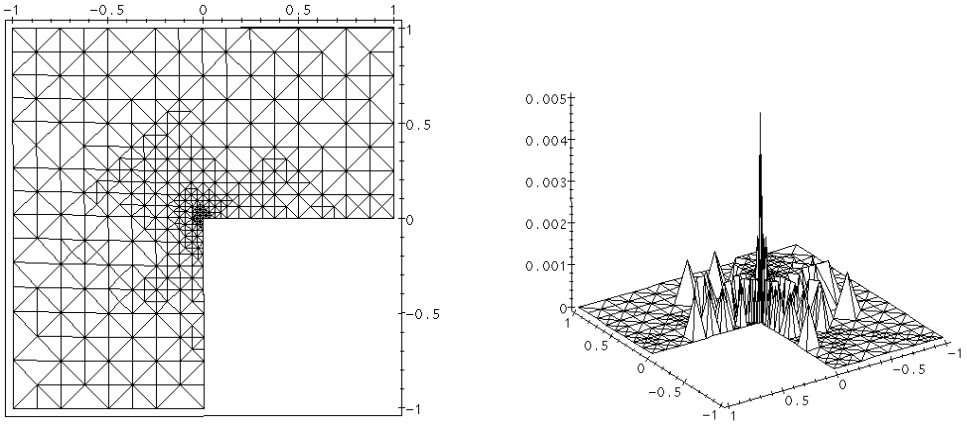

FIG. 4. *Locally refined mesh and the corresponding error after four levels of refinement.*

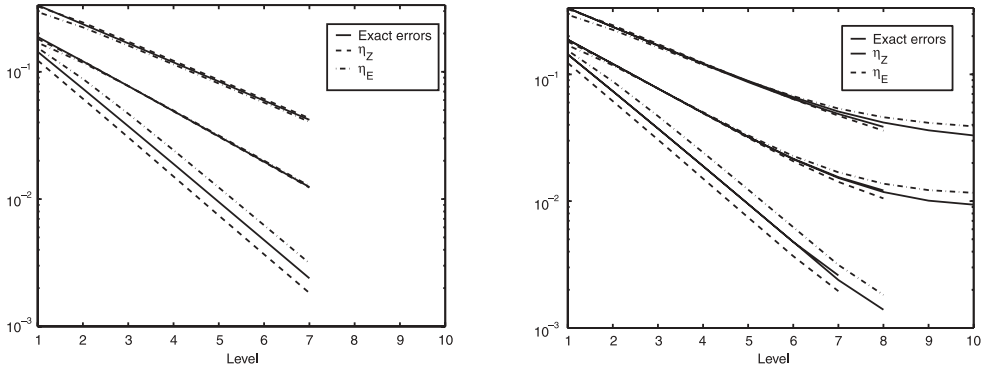

FIG. 5. *Comparison of the H^1-norm of the error for solutions $H^{1+4/3-\epsilon}$ (Problem 1), $H^{1+2/3-\epsilon}$ (Problem 2), and $H^{1+1/2-\epsilon}$ (Problem 3) on a sequence of uniformly refined grids and for grids refined locally by using the a posteriori error estimates. Left: Exact error, η_Z, and η_E for uniformly refined grids. Right: Exact error, η_Z, and η_E for locally refined grids.*

The error tolerances supplied to the refinement procedures are 0.0026 for Problem 1, 0.0122 for Problem 2, and 0.0385 for Problem 3. These are the exact errors for the problems considered on level 7 of the uniformly refined mesh. The result shows that, on the locally refined meshes, as in the uniform refinement case, both η_Z and η_E are equivalent to the exact error. Another observation is that, although the meshes are refined, only locally is the rate of error reduction over the refinement levels the same as on the uniformly refined meshes (compare the error reduction slopes with the ones in Figure 5, left).

Finally, we demonstrate the efficiency of the adaptive error control by giving the number of the degrees of freedom (DOF) on the locally refined mesh levels from Figure 5, right, and comparing them with the number of DOF on the uniformly refined mesh levels (see Table 5.1). Note the difference in the order of the mesh sizes for uniform refinement and local refinement for Problems 2 and 3. For Problem 1 we have full elliptic regularity, and η_Z/η_E are supposed to lead to uniform refinement, which is confirmed by the numerical experiment. The results demonstrate the efficiency of

TABLE 5.1

Number of DOF for the levels resulting from local refinement based on the η_Z and η_E error estimators. The error tolerances supplied to the refinement procedures are 0.0026 *for Problem* 1, 0.0122 *for Problem* 2, *and* 0.0385 *for Problem* 3 (*see Example* 1).

Level	Uniform mesh	Problem 1		Problem 2		Problem 3	
		η_Z	η_E	η_Z	η_E	η_Z	η_E
1	65	65	65	65	65	65	65
2	255	225	225	225	225	213	175
3	833	833	833	815	805	467	375
4	3201	3201	3201	2025	2080	940	695
5	12545	12545	12545	3990	4219	1461	1033
6	49665	49665	49665	5879	6249	1889	1357
7	197633	169618	197626	7322	7815	2183	1634
8			581852	8365	9034	2508	1776
9					9793		1892
10					10097		1986

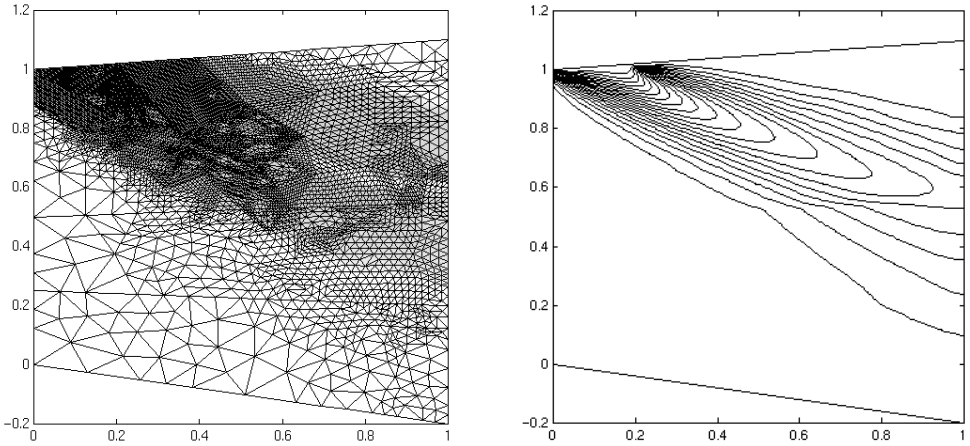

FIG. 6. *Convection-diffusion problem; the inhomogeneities are represented by three layers. Left: The locally refined mesh after four levels of adaptive refinement* (3,032 *nodes and* 5,910 *triangles*). *Right: The level curves of the solution.*

applying local refinement based on η_Z and η_E for problems with singular solutions.

Example 2. We consider problem (1.1) with Ω shown in Figure 6. In this problem Γ_D is the upper boundary, $\underline{b} = (1, -0.5)$, and $f = 0$. The domain is taken to have three layers (see Figure 6) with $A(x) = 0.01\ I$ in the top layer, $0.05\ I$ in the internal layer, and $0.001\ I$ at the bottom. The Dirichlet boundary value is 1 for $x < 0.2$ and 0 otherwise. On the Neumann boundary we take $g = 0$. In this problem we have used the upwind approximation (2.11) and the local refinement procedures based on η_Z and η_E.

Since the exact solution is not known we judge the quality of the error estimators η_Z and η_E by comparing the results with the ones on uniformly refined meshes. Also, when choosing problems with known local behavior we expect the estimators to lead to refinement that closely follows the local behavior of the solution profile. This is a standard testing approach (see, for example, [4]).

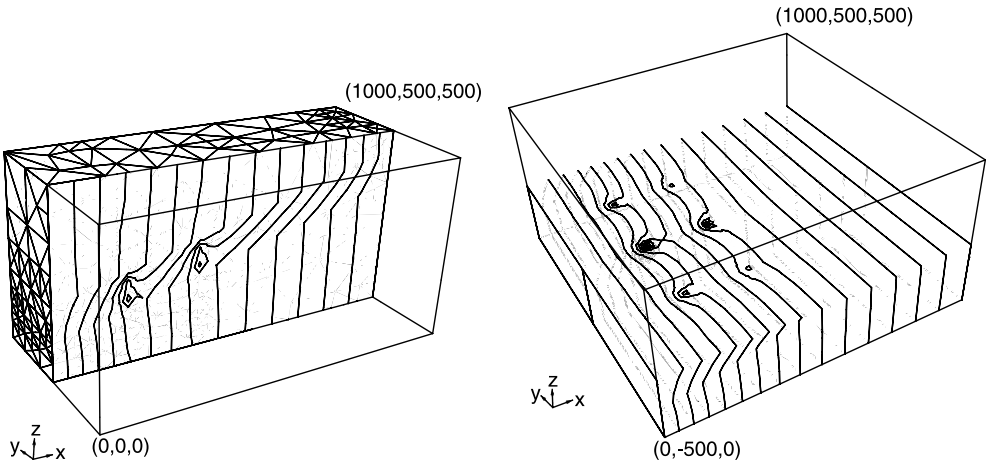

FIG. 7. *Pressure computations for a nonhomogeneous reservoir. Left: Contour curves of the pressure for the cross section* $x_2 = 250$. *Right: Contour curves of the pressure for the cross section* $x_3 = 200$.

Figure 6 shows the mesh on level 4 (left) with 3,032 nodes and 5,910 triangles. On the right are the solution level curves. This particular mesh was obtained by refinement based on η_Z with $\rho = 4\%$ of $|u_h|_1$ (≈ 0.1616, i.e., $\rho = 0.006464$). The mesh obtained by four levels of uniform refinement has 38,257 DOF. The discrete solutions have the same qualitative behavior in both cases. As expected, the mesh refinement follows the discrete solution profile. Refinement based on η_E, compared to η_Z, leads to slightly different, but qualitatively and quantitatively similar, meshes.

5.2. 3-D problems of flow and transport in porous media. This test is very similar to the 2-D Example 2. Here we test the error estimators η_Z and η_E on a real 3-D application in fluid flow and transport in porous media. Again, the exact solution is unknown but we know its local behavior, which is due to boundary layers, discontinuities of coefficients, and localized sources. The problem is described as follows.

A steady-state flow, with Darcy velocity $\underline{v}$ measured in ft/yr, has been established in a parallelepiped-shaped reservoir $\Omega = [0, 1000] \times [-500, 500] \times [0, 500]$ (see Figure 7, right). First, we determine the pressure $p(x)$ in Ω as the solution $u(x)$ of problem (1.1) with $\underline{b} = 0$, $\gamma = 0$, and $A(x) = D(x)$, where $D(x)$ is the permeability tensor. The pressure at faces $x_1 = 0$ and $x_1 = 1000$ is constant (correspondingly, 2,000 and 0). The rest of the boundary is subject to a no-flow condition. We take the permeability $D(x)$ to be 32 I everywhere in Ω except in the layer (see Figure 7, middle) where $D(x)$ is taken to be 10 times smaller than in the rest of the domain, i.e., in the layer $D(x) = 3.2\ I$.

Also, we have six production wells. For all of them x_3 is in the range $0, \ldots, 400$. Their (x_1, x_2) coordinates are correspondingly (200, -250), (400, -250), (200, 0), (400, 0), (200, 250), and (400, 250). We treat a well simply as a line-delta function (sink) along the well axis. Production rates $Q = 16{,}000$ l/yr for wells in plane $x_2 = 0$, and $Q = 8{,}000$ l/yr for the rest, are the intensities of the sink. Figure 7 shows half of the mesh and the contour curves of the pressure for the cross section $x_2 = 250$ (left) after five levels of local refinement. It has 19,850 tetrahedrons and 3,905 nodes. The right picture shows the contour curves for the cross section $x_3 = 200$.

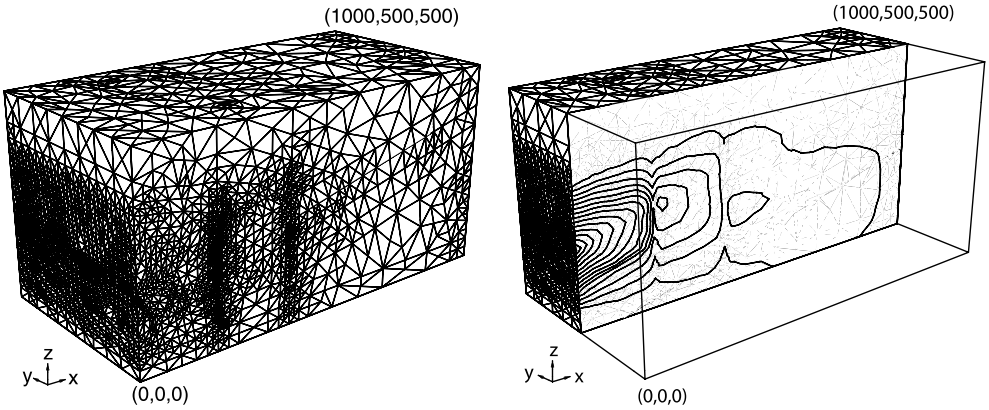

FIG. 8. *Concentration computations for a nonhomogeneous reservoir. Left: The* 3*-D mesh on refinement level* 11 *with* 219,789 *tetrahedrons and* 39,752 *nodes. Right: Concentration contour curves for cross section* $x_2 = 250$.

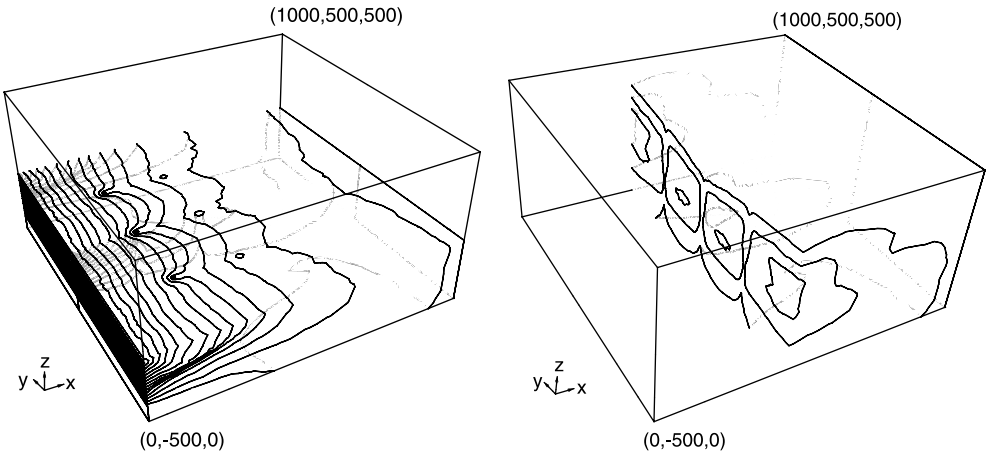

FIG. 9. *Concentration level curves at cross sections* $x_3 = 200$ (*left*) *and* $x_1 = 400$ (*right*).

The weighted pressure gradient $-D\nabla p$ forces the groundwater to flow. The transport of a contaminant dissolved in the water (in our case, benzene) is described by the convection-diffusion-reaction equation (1.1), where $u(x)$ represents the benzene concentration, $\underline{b}$ is the Darcy velocity $\underline{v} = -D\nabla p$, γ is the biodegradation rate, and $A(x)$ is the diffusion-dispersion tensor:

$$A(x) = k_{\text{diff}} I + k_t \underline{v}^T \underline{v}/|\underline{v}| + k_l(|\underline{v}|^2 I - \underline{v}^T \underline{v})/|\underline{v}|.$$

Here $k_{\text{diff}} = 0.0001$, $k_t = 21$, and $k_l = 2.1$ are the coefficients of diffusion, transverse, and longitudinal dispersions, respectively. A steady piecewise linear in x_3 and constant in x_2 leakage of benzene of maximum 30 mg/l is applied on the boundary strip $x_1 = 0$ and $50 \le x_3 \le 350$. The leakage is 30 mg/l at $x_3 = 200$ and drops linearly to 0 at $x_3 =$ 50 and 350. The rest of the boundary is subject to a homogeneous Neumann boundary condition. The dispersion/convection process causes the dissolved benzene to disperse in the reservoir. The biodegradation transforms it into a solid substance which is absorbed by the soil. This leads to a decrease in the benzene. The computations are

for the case of low absorption rate $\gamma = 0.05$. We approximate the convection term using the upwind approximation (2.10).

Figure 8 shows the obtained mesh in half of the domain (left) on refinement level 11. The mesh has 219,789 tetrahedrons and 39,752 nodes. The first five level of refinement are for the pressure equation, the rest for the concentration. Figure 8 (right) shows the level curves for the concentration in the reservoir cross section $x_2 = 250$ on the same refinement level. Figure 9 gives the level curves at two more cross sections, $x_3 = 200$ (left) and $x_1 = 400$ (right).

REFERENCES

[1] R. A. Adams, *Sobolev Spaces*, Academic Press, New York, 1975.

[2] L. Angermann, *Balanced a posteriori error estimates for finite-volume type discretizations of convection-dominated elliptic problems*, Computing, 55 (1995), pp. 305–324.

[3] L. Angermann, *An a-posteriori estimation for the solution of an elliptic singularly perturbed problem*, IMA J. Numer. Anal., 12 (1992), pp. 201–215.

[4] L. Angermann, P. Knabner, and K. Thiele, *An error estimator for a finite volume discretization of density driven flow in porous media*, Appl. Numer. Math., 26 (1998), pp. 179–191.

[5] D. N. Arnold, A. Mukherjee, and L. Pouly, *Locally adapted tetrahedral meshes using bisection*, SIAM J. Sci. Comput., 22 (2000), pp. 431–448.

[6] I. Babuška and W. C. Rheinboldt, *Error estimates for adaptive finite element computations*, SIAM J. Numer. Anal., 15 (1978), pp. 736–754.

[7] I. Babuska and T. Strouboulis, *The Finite Element Method and Its Reliability*, Oxford University Press, London, 2001.

[8] R. E. Bank and D. J. Rose, *Some error estimates for the box method*, SIAM J. Numer. Anal., 24 (1987), pp. 777–787.

[9] R. E. Bank and R. K. Smith, *A posteriori error estimates based on hierarchical bases*, SIAM J. Numer. Anal., 30 (1993), pp. 921–935.

[10] S. Bartels and C. Carstensen, *Each averaging technique yields reliable a posteriori error control in FEM on unstructured grids. Part* II: *Higher order FEM*, Math. Comp., 71 (2002), pp. 971–994.

[11] R. Becker and R. Rannacher, *A feed-back approach to error control in finite element methods: Basic analysis and examples*, East-West J. Numer. Math., 4 (1996), pp. 237–264.

[12] S. C. Brenner and L. R. Scott, *The Mathematical Theory of Finite Element Methods*, 2nd ed., Springer-Verlag, New York, 2002.

[13] Z. Cai, *On the finite volume element method*, Numer. Math., 58 (1991), pp. 713–735.

[14] C. Carstensen and S. Bartels, *Each averaging technique yields reliable a posteriori error control in FEM on unstructured grids. Part* I: *Low order conforming, nonconforming, and mixed FEM*, Math. Comp., 71 (2002), pp. 945–969.

[15] C. Carstensen and S. A. Funken, *Constants in Clément-interpolation error and residual-based a posteriori estimates in finite element methods*, East-West J. Numer. Anal., 8 (2000), pp. 153–175.

[16] C. Carstensen and S. A. Funken, *Fully reliable localized error control in the FEM*, SIAM J. Sci. Comput., 21 (2000), pp. 1465–1484.

[17] C. Carstensen and S. A. Funken, *A posteriori error control in low-order finite element discretizations of incompressible stationary flow problems*, Math. Comp., 70 (2001), pp. 1353–1381.

[18] S. H. Chou and Q. Li, *Error estimates in L^2, H^1, and L^∞ in covolume methods for elliptic and parabolic problems: A unified approach*, Math. Comp., 69 (2000), pp. 103–120.

[19] G. Dagan, *Flow and Transport in Porous Formations*, Springer-Verlag, Berlin, Heidelberg, 1989.

[20] W. Dörfler and O. Wilderotter, *An adaptive finite element method for a linear elliptic equation with variable coefficients*, ZAMM Z. Angew. Math. Mech., 80 (2000), pp. 481–491.

[21] K. Eriksson, D. Estep, P. Hansbo, and C. Johnson, *Computational Differential Equations*, Cambridge University Press, Cambridge, UK, 1996.

[22] K. Eriksson and C. Johnson, *An adaptive finite element method for linear elliptic problems*, Math. Comp., 50 (1988), pp. 361–382.

[23] R. Eymard, T. Gallouët, and R. Herbin, *Finite Volume Methods*, in Handbook of Numerical Analysis VII, North-Holland, Amsterdam, 2000, pp. 713–1020.
[24] T. Ikeda, *Maximum Principle in Finite Element Models for Convection-Diffusion Phenomena*, Lecture Notes in Numer. Appl. Anal. 4, North-Holland Math. Stud. 6, Kinokuniya Book Store Co., Ltd., Tokyo, 1983.
[25] R. D. Lazarov and S. Z. Tomov, *A posteriori error estimates for finite volume element approximations of convection-diffusion-reaction equations*, Comput. Geosci., 6 (2002), pp. 483–503. Available online at http://www.isc.tamu.edu/iscpubs/0107.ps.
[26] R. H. Li, Z. Y. Chen, and W. Wu, *Generalized Difference Method for Differential Equations. Numerical Analysis of Finite Volume Methods*, Marcel Dekker, Inc., New York, Basel, 2000.
[27] I. D. Mishev, *Finite volume methods on Voronoi meshes*, Numer. Methods Partial Differential Equations, 14 (1998), pp. 193–212.
[28] L. Oganesian and V. L. Ruhovetz, *Variational-Difference Methods for Solving Elliptic Equations*, Publishing House of Armenian Academy of Sciences, Erevan, Armenia, 1979.
[29] A. Quarteroni and A. Valli, *Domain Decomposition Methods for Partial Differential Equations*, Clarendon Press, Oxford, UK, 1999.
[30] R. Rodriguez, *Some remarks on Zienkiewicz-Zhu estimator*, Numer. Methods Partial Differential Equations, 10 (1994), pp. 625–635.
[31] H.-O. Ross, M. Stynes, and L. Tobiska, *Numerical Methods for Singularly Perturbed Differential Equations*, Springer-Verlag, Berlin, 1996.
[32] R. Rannacher and R. Scott, *Some optimal error estimates for piecewise linear element approximations*, Math. Comp., 38 (1982), pp. 437–445.
[33] A. A. Samarskii, *The Theory of Difference Schemes*, Marcel Dekker, Inc., New York, 2001.
[34] M. Tabata, *A finite element approximation corresponding to the upwind finite differencing*, Mem. Numer. Math., 4 (1977), pp. 47–63.
[35] K. Thiele, *Adaptive Finite Volume Discretization of Density Driven Flows in Porous Media*, Ph.D. Dissertation, Naturwissenschaftliche Facultät I, Universität Erlangen-Nürnberg, Nuremberg, Germany, 1999.
[36] R. Verfürth, *A posteriori error estimation and adaptive mesh-refinement techniques*, J. Comput. Appl. Math., 50 (1994), pp. 67–83.
[37] O. C. Zienkiewicz and J. Z. Zhu, *A simple error estimator and adaptive procedure for practical engineering analysis*, Int. J. Numer. Methods Engrg., 24 (1987), pp. 337–357.
[38] O. C. Zienkiewicz and J. Z. Zhu, *Adaptivity and mesh generation*, Int. J. Numer. Methods Engrg., 32 (1991), pp. 783–810.